Ferrofluid Dynamics In a Hele-Shaw Cell Simultaneously Stressed by DC and Rotating Magnetic Fields

by

Uzoma A. Orji

B.S., Electrical Engineering (2006)
Massachusetts Institute of Technology

Submitted to the Department of Electrical Engineering and Computer Science
in partial fulfillment of the requirements for the degree of

Master of Engineering in Electrical Engineering

at the

MASSACHUSETTS INSTITUTE OF TECHNOLOGY

June 2007

© Uzoma A. Orji, MMVII. All rights reserved.

The author hereby grants to MIT permission to reproduce and distribute publicly paper and electronic copies of this thesis document in whole or in part.

Author .....
Department of Electrical Engineering and Computer Science
May 18, 2007

Certified by .....
Markus Zahn
Professor of Electrical Engineering
Thesis Supervisor

Accepted by .....
Arthur C. Smith
Chairman, Department Committee on Graduate Students

MASSACHUSETTS INSTITUTE OF TECHNOLOGY
OCT 0 3 2007
LIBRARIES

ARCHIVES

Ferrofluid Dynamics In a Hele-Shaw Cell Simultaneously Stressed by DC and Rotating Magnetic Fields

by

Uzoma A. Orji

Submitted to the Department of Electrical Engineering and Computer Science
on May 18, 2007, in partial fulfillment of the
requirements for the degree of
Master of Engineering in Electrical Engineering

Abstract

Earlier experiments have been repeated to evaluate magnetic fluid behavior in DC, AC and rotating magnetic fields. Understanding these behaviors are essential to the ferrohydrodynamic applications of ferrofluids in biomedicine. Careful measurements in Hele-Shaw cells with simultaneous perpendicular DC and in-plane rotating magnetic fields have shown that ferrofluid drop spiral patterns rotate in the same direction as the rotating magnetic field, independent of the polarity of the perpendicular DC magnetic field. This corrects inconsistencies in previously reported measurements. The large and heavy electromagnet and power supply used in earlier work were also replaced by a small permanent magnet assembly from Magswitch™ to still produce ferrofluid spirals and spontaneous self-assembling ferrofluid dot patterns.

Thesis Supervisor: Markus Zahn
Title: Professor of Electrical Engineering

Acknowledgments

I would like to thank my thesis supervisor, Markus Zahn, for mentoring me and sharing his knowledge with me. Many thanks go to Wayne Ryan, our lab technician, for helping me with constructing cells and serving as a valuable resource. To all the students at the High Voltage Research Laboratory (HVRL) - Shihab Elborai, Tony He, Zachary Thomas and Clinton Lawler - I express sincere gratitude for all the help.

I would like to thank Dr. K. Raj of Ferrotec^{TM} for supplying the display cell ferrofluid for use in this thesis and to Franz Kocijan and Nathan Williams of Magswitch^{TM}for supplying a Magswitch magnet for use in my research.

On a personal note, I wish to send a big shout out to my family. All this would not have been possible without my parents preaching the value of a good education. I should thank my two brothers and my sister - as foolish as they are - for years and years of raucous behavior growing up.

This research was supported by a grant from United States National Science Foundation (NSF) Graduate Research Fellowship Program and by a grant from the United States-Israel Binational Science Foundation (BSF), Jerusalem, Israel (Grant # 2004081).

Contents

List of Figures

List of Tables

Chapter 1

Introduction

Magnetic fluids, also known as ferrofluids, are mixtures typically containing water or oil combined with permanently magnetized particles. These particles, usually magnetite, have diameters on the order of 10nm and make up about 3-10% of the volume of the ferrofluid [1]. Because of the small particle size, the study of ferrofluids includes nanoscience and nanotechnology. Current research on ferrofluids focuses on the synthesis and characterization of the nanoparticles for multiple applications. The most notable applications include using these particles in electromechanical sensors, actuators and nanofluidic devices [1]. They are also being applied in biomedical applications for targeted drug-delivery, hyperthermia and magnetic resonance imaging (MRI) [2].

1.1 Ferrofluids

Understanding how ferrofluids respond under magnetic fields is essential for its biomedicine applications. Ferrofluids have the potential to designate target sites for efficient drug delivery. Cytotoxic drugs can be attached to the magnetic nanoparticles in the ferrofluids before being injected into a patient. An external magnetic field can be applied near the target site of the patient to direct the drugs to the correct area of the body. Hyperthermia can then be applied to kill cancerous tumors. Once the nanoparticles are delivered to a target site of

cancerous cells, they can be heated by an external magnetic field thereby destroying nearby tumors [2].

Ferrofluids are also being used for MRI contrast enhancement. An MRI image contrast is possible because tissues in the body have different T1 and T2 relaxation times [3]. T1 is the time it takes for proton magnetization to align with the external field after radio frequency (RF) excitation. T2 is the time for transverse magnetization to decay after the RF pulse is removed . By applying an external rotating magnetic field to a ferrofluid, the rotating field can actuate a spin of the magnetic nanoparticles which alters the complex magnetic susceptibility (CMS) tensor of the ferrofluid [4]. Changing the CMS tensor of the ferrofluid temporally modulates the MRI signal intensity. The resulting "twinkling" MRI image makes it easier to locate the magnetic nanoparticles.

1.2 Scope of Thesis

Chapter 2 provides results of experiments used to resolve earlier discrepancies from previous research. Ferrofluid spirals are formed when excited under an axial DC magnetic field. When an in-plane rotating magnetic field is then turned on, these spirals curl either clockwise or counterclockwise. It is uncertain whether the spirals curl in the same or opposite direction to the rotating magnetic field. It also unclear if the polarity of the axial field has any effect on the direction in which the spirals curl. Similar experiments are repeated to resolve these uncertainties.

Chapter 3 discusses using a Magswitch magnet to produce the axial DC magnetic field to obtain a more portable experiment setup. The experiments conducted in chapter 2 used heavy, non-portable equipment. The use of the Magswitch magnet makes the system more portable. Measurements are taken to obtain a profile of the three dimensional magnetic field of the magnet. Experiments are also conducted with the Magswitch to produce the same results as previous setups.

Chapter 4 displays the images obtained with the Magswitch and the stator coil winding. Pictures are displayed which show both the curling spirals and phase transitions. Chapter

5 includes a summary of the results obtained in this thesis and a brief discussion of possible future work.

Chapter 2

Determining Ferrofluid Spin Orientation

2.1 Previous Research

The research being done at the Laboratory of Electromagnetic and Electrical Systems aims to understand the role of ferrofluid nanoparticle spin velocity. Previous experiments have been conducted which analyze instabilities of a ferrofluid drop in a Hele-Shaw cell [5] under the presence of axial and rotating magnetic fields. A Hele-Shaw cell has a thin gap between two glass plates. A ferrofluid drop in the gap is surrounded by a non-magnetic fluid solution that is 50% propyl alcohol and 50% deionized water, known as propanol, to prevent the ferrofluid from sticking to the glass plates. The Hele-Shaw cell used in this thesis was 2.5 inches in diameter with a 0.9 mm gap. Ferrotec provided the fluorocarbon-based display cell ferrofluid used in these experiements.

The results have shown that the droplet forms a labyrinth pattern when stressed by a uniform DC axial field. This phenomenon is shown in Figure 2-1(a) [6]. When an in-plane rotating field is later applied, the labyrinth pattern curls to form spirals as shown in Figure 2-1(b). The experiment was repeated by applying the rotating field before the DC axial field is applied. The rotating field holds the drop together without the formation of a labyrinth.

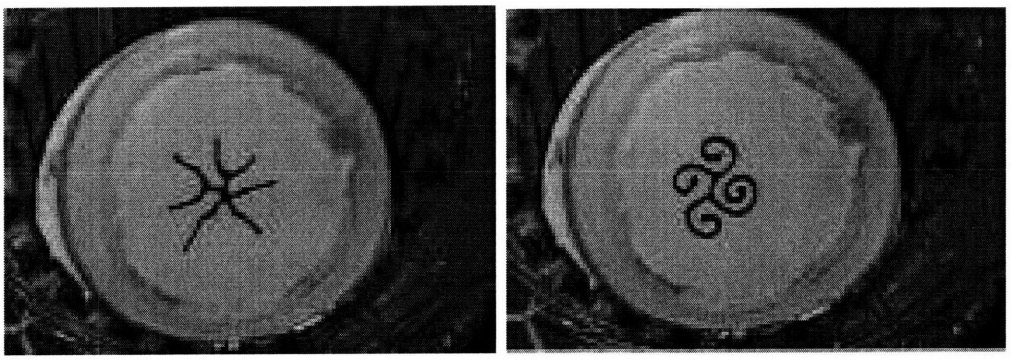

(a) Labyrinth pattern forms under an axial DC magnetic field.

(b) Labyrinth curls in the counter-clockwise direction when an in-plane counter-clockwise rotating field is applied.

Figure 2-1: Ferrofluid labyrinth patterns with (a) an axial magnetic DC field applied first and then (b) an in-plane rotating magnetic field applied [5]. The direction of the spiral is in the same direction as the rotating magnetic field independent of the polarity of the axial DC magnetic field.

With the application of the perpendicular magnetic field, at a critical strength, a pattern of smaller droplets spontaneously form [6]. Figure 2-2 shows this spontaneous phase transition.

2.1.1 Earlier Contradictions

In Figure 2-2, the spirals can curl in either a clockwise or counterclockwise direction. The direction of the spirals with respect to the rotation of direction of the AC rotating field was uncertain from previous research. One study [5] claimed that the spirals curled in the opposing direction of the rotating magnetic field. If the rotating field is oriented clockwise, the study claimed that the ferrofluid curled counterclockwise and vice versa. Another study [6] stated that the ferrofluid curls in the same direction of the rotating field. So, the spirals would curl clockwise under a clockwise rotating field and vice versa.

The cause of the reported discrepancy is unknown. One possibility could be that during one of the studies, the direction of the rotating field was not verified with a compass and was erroneously assumed. One other cause could be that the direction of the axial field affects the direction of the curl depending on whether it is directed into or out of the plane of the ferrofluid. Perhaps, both studies had axial fields in different direction and this difference was

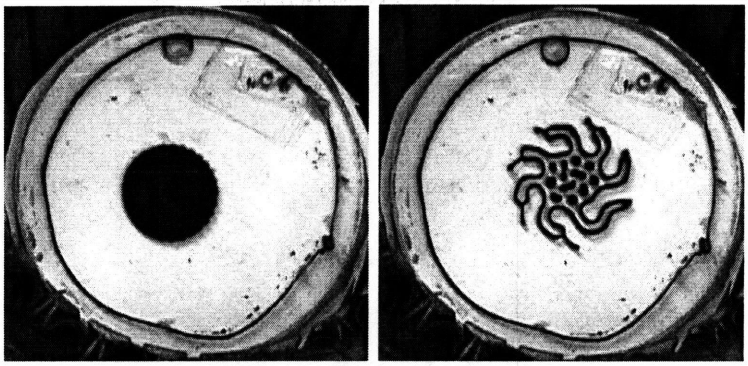

(a) The drop holds its circular shape in the rotating magnetic field.

(b) Phase transition under a DC axial field.

Figure 2-2: Ferrofluid phase transition with (a) an in-plane rotating magnetic field applied first and then (b) a DC axial magnetic field is applied.

the source of the discrepancy. Perhaps, one report was simply wrong.

This project repeats the experiments with the DC axial magnetic field applied before the AC rotating field to determine that the spiral curls are in the same direction as the rotating field independent of the polarity of the vertical DC magnetic field. For both clockwise and counterclockwise directions of the rotating field, experiments were conducted with both directions of the DC field to determine that the polarity of the DC field has no effect on the spiral curls of the ferrofluid. The same procedure is repeated with the AC rotating field applied before the DC axial magnetic field to reproduce the phase transitions of the ferrofluid.

2.2 Experiment Setup

To conduct these experiments, a DC axial and AC in-plane rotating magnetic field need to be applied to the ferrofluid. This is done by placing a cylindrical motor stator winding inside a solenoidal electromagnet. Figure 2-3 shows the actual motor stator and the electromagnet.

To produce the rotating magnetic field, current is supplied to two of the three windings of the cylindrical motor stator. The third winding is grounded. To produce balanced three

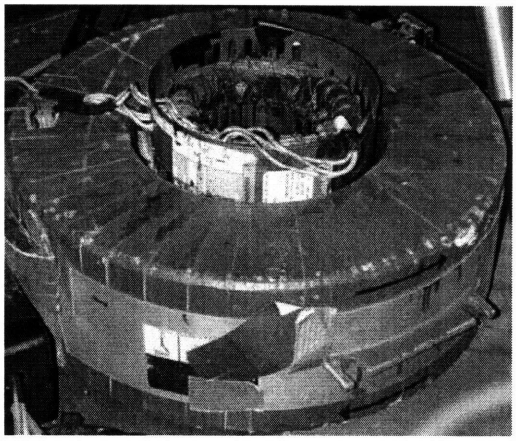

Figure 2-3: Cylindrical motor stator winding inside a toroidal DC electromagnet.

phase AC in the stator windings, the two windings must be $\pm 60°$ out of phase with each other. The $+60°$ phase difference gives a clockwise rotating magnetic field and -60° phase difference gives a counterclockwise rotating magnetic field. The two activated windings have the same sinusoidal currents with amplitudes up to 5A peak at the same frequency over the range of 20-35 Hz. For the labyrinth patterns, the stator winding currents typically have a frequency of 20 Hz. For the phase transitions, the stator winding currents typically have a frequency of 30 Hz. The sinusoidal currents are generated by a Wavetek 40 MS/s Universal Wave Generator. An AE Techron 5050 Linear Amplifier amplifies the signal before they are supplied to the windings of the motor stator. This lab apparatus is shown in Figure 2-4.

Figure 2-4: Waveform generator and Linear amplifier.

Three Fluke 45 Dual Display Multimeters, shown in Figure 2-5, are each placed in series

with each of the three phase windings to measure the current to ensure that each winding was carrying the same amplitude current. Once the in-plane AC rotating field was established, the DC axial field is produced. To produce the DC axial field, the solenoidal magnet is driven by a DC current from a large DC power supply shown in Figure 2-6.

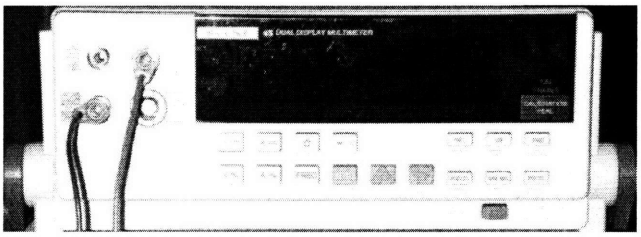

Figure 2-5: Multimeters used to measure AC current.

The windings around the magnet produce a uniform axial field in the center of the solenoid. The DC power supply in Figure 2-6 has a Variac controlled autotransformer which supplies the DC current that drives the solenoidal electromagnet.

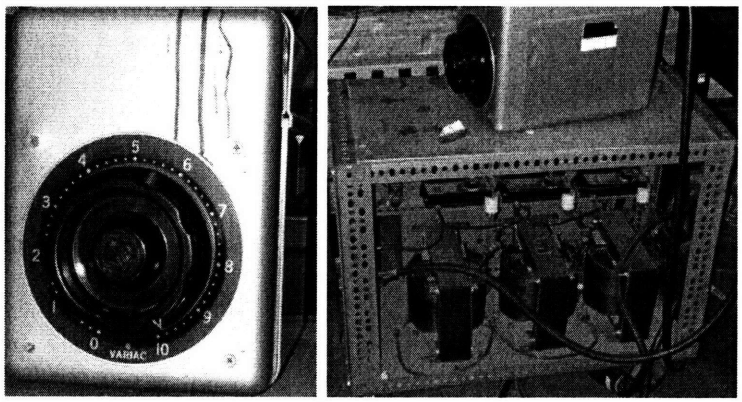

(a) (b)

Figure 2-6: Variac Autotransformer DC power supply that drives the DC solenoidal coil in Figure 2-3.

The applied in-plane AC rotating field is produced by currents in the stator windings in Figure 2-3. Each 1 A rms in the three phases gives approximately 38 Gauss (rms) in the central region of the stator [6]. The DC axial field was measured in the center of the solenoid with the F.W. Bell Model 7030 Gauss/Teslameter as shown in Figure 2-7. Each 1 A DC gives about 5-6 Gauss.

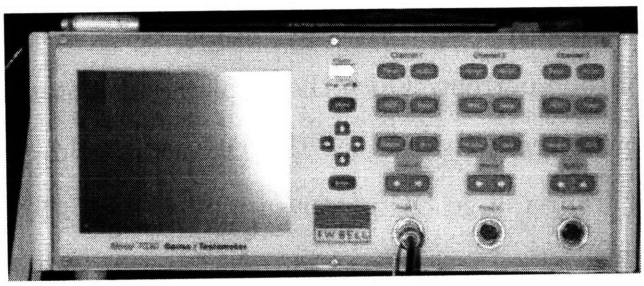

Figure 2-7: Teslameter

If the measured magnetic field is negative, then the field is directed into the axis of the axial probe. The probe is placed downward at the center of the toroid magnet. Therefore, a negative field means the field is directed upwards. Similarly, a positive field is directed downwards. The results for the experiments conducted are discussed in the next section.

2.3 Measured Ferrohydrodynamic Patterns

In this section, the results for labyrinth patterns and phase transitions are presented.

2.3.1 Labyrinth Spirals

The DC axial field is slowly increased to the typical range between 84 - 92 Gauss when the ferrofluid takes the shape of a labyrinth. The in-plane AC rotating magnetic field is then turned on which causes the labyrinth to form spirals. The rotating AC magnetic field typically has a frequency of 20 Hz and amplitudes of about 15.5 Gauss(rms). In all cases, these spirals rotate in the direction of the rotating magnetic field, independent of the DC magnetic field polarity.

Figures 2-8 to 2-11 show representative spiral patterns and the directions in which the spirals curl.

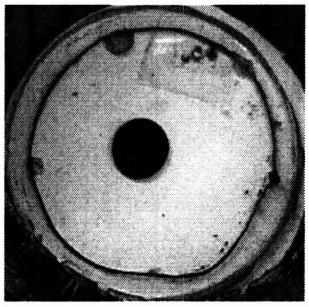

(a) Ferrofluid drop with no applied magnetic field

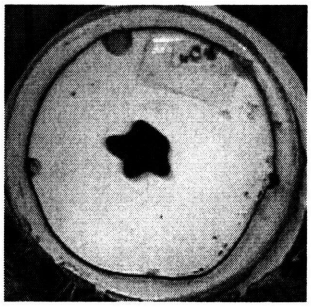

(b) +78 Gauss DC On

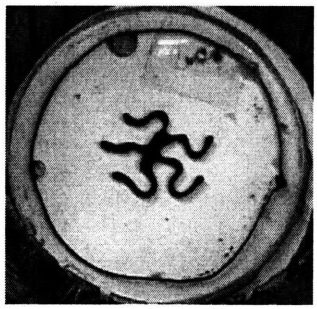

(c) +84 Gauss DC

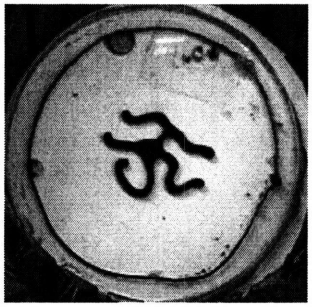

(d) 20 Hz, 15.6 Gauss (rms) CW AC turned on

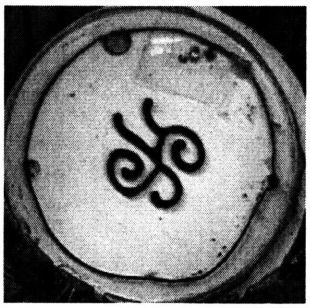

(e) Labyrinth curls in direction of rotating AC field

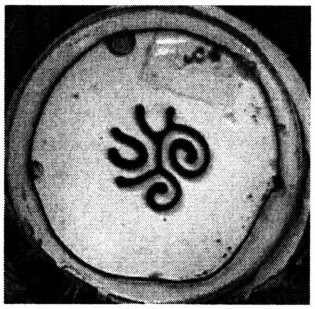

(f) Spirals of labyrinth pattern

Figure 2-8: Labyrinth pattern for positive (downwards) DC field and clockwise rotating AC field. The DC axial magnetic field is increased to the value given in the corresponding picture. The clockwise AC field, fixed at 20 Hz and 15.6 Gauss (rms), is then turned on. The labyrinth spirals curl in the direction of the AC rotating field.

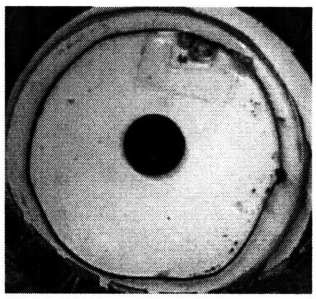

(a) Ferrofluid drop with no applied magnetic field

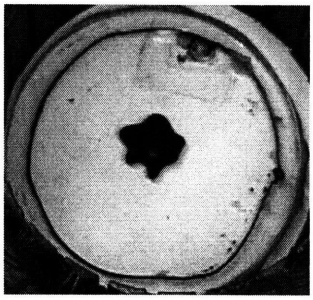

(b) +78 Gauss DC On

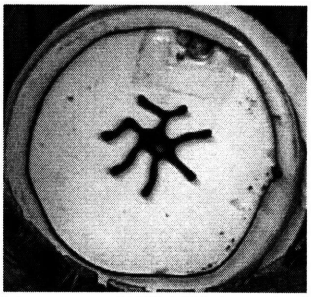

(c) +84 Gauss DC

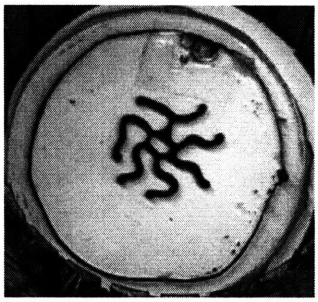

(d) 20 Hz, 15.2 Gauss (rms) CCW AC turned on

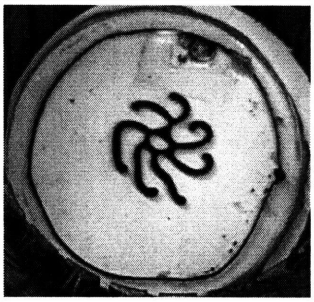

(e) Labyrinth curls in direction of rotating AC field

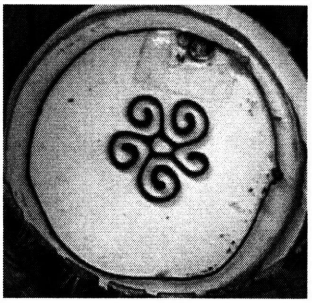

(f) Spirals of labyrinth pattern

Figure 2-9: Labyrinth pattern for positive (downwards) DC field and counterclockwise rotating AC field. The DC axial magnetic field is increased to the value given in the corresponding picture. The counterclockwise AC field, fixed at 20 Hz and 15.2 Gauss (rms), is then turned on. The labyrinth spirals curl counterclockwise.

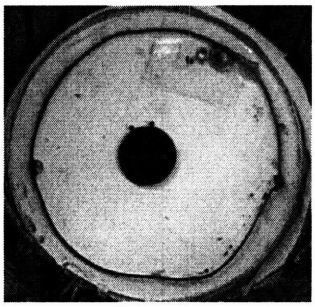

(a) Ferrofluid drop with no applied magnetic field

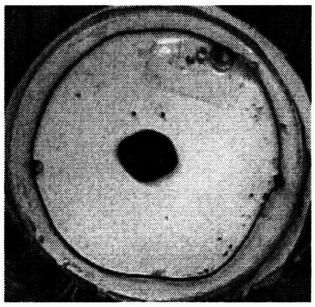

(b) -66 Gauss DC On

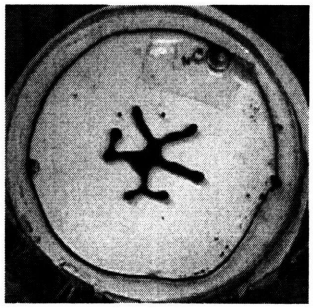

(c) -84 Gauss DC

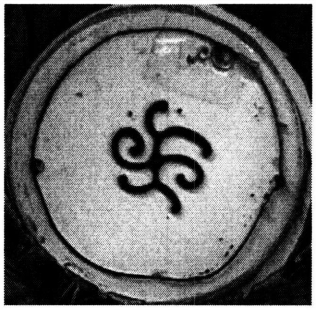

(d) 20 Hz, 15.7 Gauss (rms) CW AC turned on

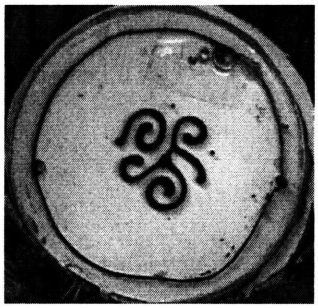

(e) Labyrinth curls in direction of rotating AC field

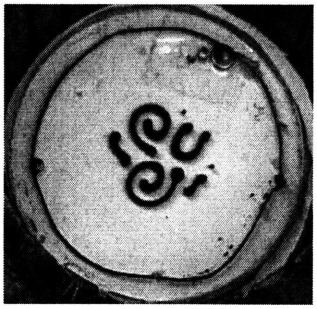

(f) Spirals of labyrinth pattern

Figure 2-10: Labyrinth pattern for negative (upwards) DC field and clockwise rotating AC field. The DC axial magnetic field is increased to the value given in the corresponding picture. The clockwise AC field, fixed at 20 Hz and 15.7 Gauss (rms), is then turned on. The labyrinth spirals curl in the direction of the AC rotating field.

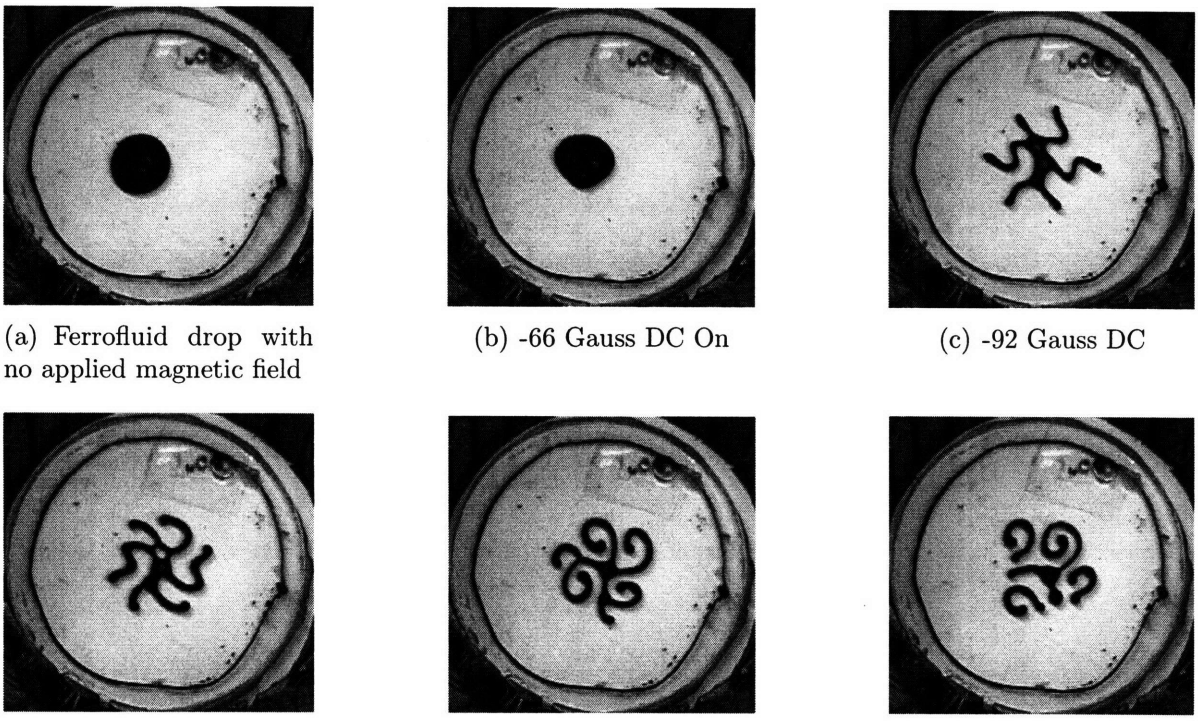

(a) Ferrofluid drop with no applied magnetic field

(b) -66 Gauss DC On

(c) -92 Gauss DC

(d) 20 Hz, 15.4 Gauss (rms) CCW AC turned on

(e) Labyrinth curls in direction of rotating AC field

(f) Spirals of labyrinth pattern

Figure 2-11: Labyrinth pattern for negative (upwards) DC field and counterclockwise rotating AC field. The DC axial magnetic field is increased to the value given in the corresponding picture. The counterclockwise AC field, fixed at 20 Hz and 15.4 Gauss (rms), is then turned on. The labyrinth spirals curl counterclockwise.

2.3.2 Phase Transitions

In this section, phase transitions are discussed for an applied 30 Hz AC rotating field with amplitude on the order of 22 Gauss (rms). The results are shown for both clockwise and counterclockwise AC rotating fields each followed by a positively and negatively directed DC axial field. In all cases, the spirals rotate in the direction of the rotating magnetic field, independent of the DC magnetic field.

Figures 2-12 to 2-15 show the phase transitions and the directions in which the spirals curl.

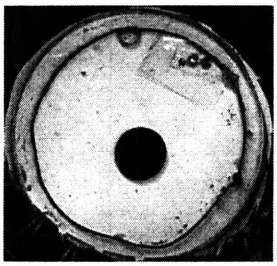

(a) Ferrofluid drop with no applied magnetic field

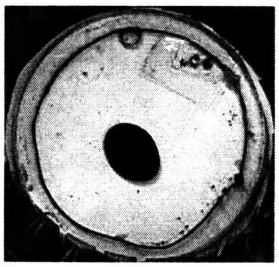

(b) 30 Hz, 21.9 Gauss (rms) CW AC On

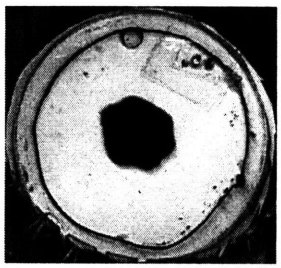

(c) +107 Gauss DC On

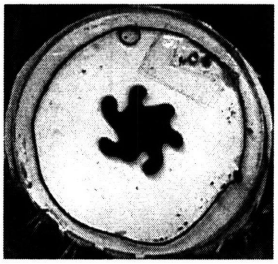

(d) +122 Gauss DC

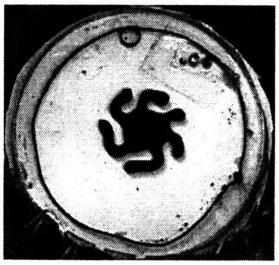

(e) +132 Gauss DC

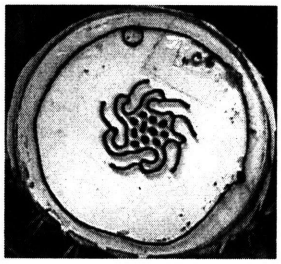

(f) +144 Gauss DC

Figure 2-12: Phase Transformations for clockwise rotating AC field and positive DC field. The AC field is fixed at 30 Hz and 21.9 Gauss (rms) and the DC axial magnetic is increased to the value shown in the corresponding picture. Note that the spirals curl in the direction of the AC rotating field.

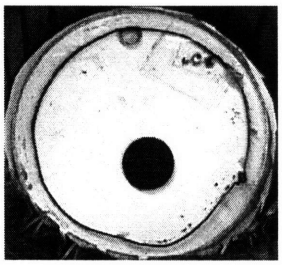

(a) Ferrofluid drop with no applied magnetic field

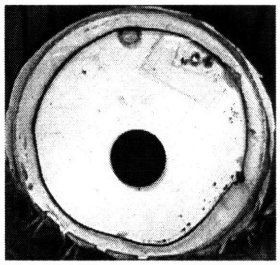

(b) 30 Hz, 21.2 Gauss (rms) CCW AC On

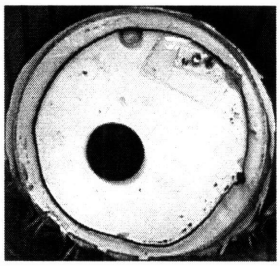

(c) +53 Gauss DC On

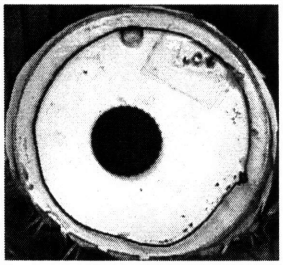

(d) +84 Gauss DC

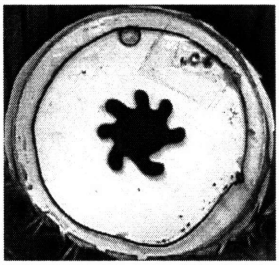

(e) +107 Gauss DC

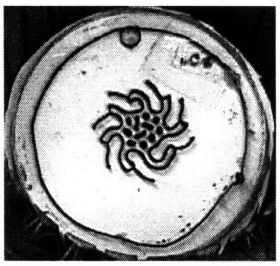

(f) +144 Gauss DC

Figure 2-13: Phase Transformations for counterclockwise rotating AC field and positive DC field. Note that the spirals curl counterclockwise, opposite to that of the spirals formed under a clockwise rotating AC field in Figure 2-12.

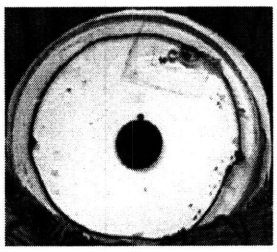

(a) Ferrofluid drop with no applied magnetic field

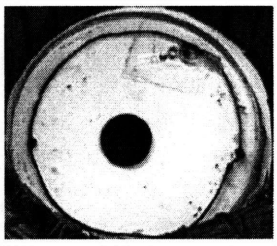

(b) 30 Hz, 19.6 Gauss (rms) CW AC On

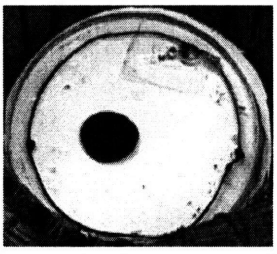

(c) -53 Gauss DC On

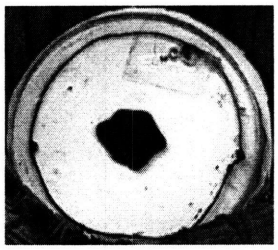

(d) -92 Gauss DC

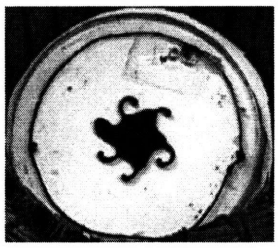

(e) -107 Gauss DC

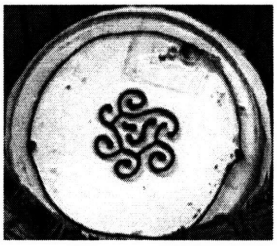

(f) -115 Gauss DC

Figure 2-14: Phase Transformations for clockwise rotating AC field and negative (upwards) DC field. Note that the spirals curl in the direction of the AC field as in Figure 2-12. The direction of the DC axial field has no effect on the spirals.

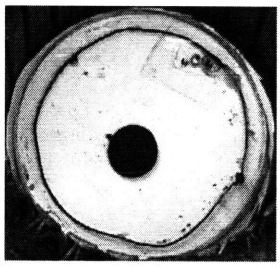

(a) Ferrofluid drop with no applied magnetic field

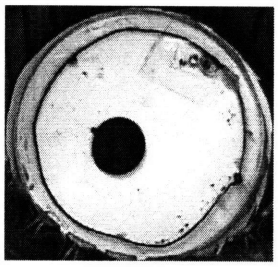

(b) 30 Hz, 22.1 Gauss (rms) CCW AC On

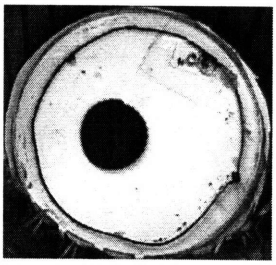

(c) -53 Gauss DC On

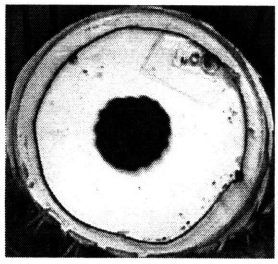

(d) -92 Gauss DC

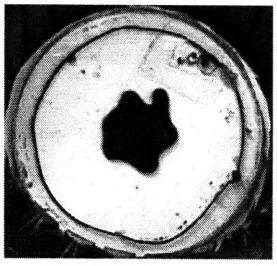

(e) -107 Gauss DC

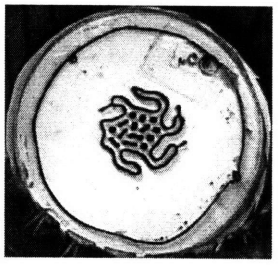

(f) -144 Gauss DC

Figure 2-15: Phase Transformations for counterclockwise rotating AC field and negative (upwards) DC field.

2.4 Discussion

This set of measurements has resolved the discrepancy in previously reported measurements [1][6] of spiral curl with respect to direction of in-plane rotating AC magnetic field and DC axial magnetic field polarity. A ferrofluid drop forms labyrinth patterns when a vertical DC axial field is applied to it. It then curls to form spirals when an in-plane AC rotating magnetic field is applied. Spirals form that curl in the same direction as the rotating magnetic field. A ferrofluid drop undergoes a phase transition when an in-plane AC rotating magnetic field is first applied followed by an axial DC field. The results shown in this report conclude that the spirals always curl in the direction of the applied rotating field with the direction of the DC axial field having no effect on the direction of the curls.

Chapter 3

Magswitch Magnet

3.1 Description of Magswitch Magnet

The second goal of this thesis research is to produce similar ferrofluid spirals and dot-like patterns as those from previous research but with a smaller experiment setup. By using smaller components, a portable version of the experiment may be constructed. The first step in creating a portable setup will be finding new compact ways to produce a DC axial magnetic field. Magswitch^{TM} is a company based in Australia [7] that specializes in "non-electric switching magnet technology." Specifically, they produce small permanent magnet devices in which the user can increase the strength of the magnetic field from zero by turning a knob. Figure 3-1 shows the magnet which Magswitch donated for this research.

When the red dial on the side face is pointed toward the bottom, the magnetic field is off or very small. When the dial is pointed upward, the magnetic field is at a maximum. This small device essentially replaces the large cart containing the the solenoidal magnet and the Variac autotransformer shown in Figures 2-3 and 2-6, respectively. Moreover, the Magswitch magnet requires no power and fits right in the user's hand. Its dimensions in inches are 2.5 x 2.5 x 2.375. Figures 3-2 provides alternate views of the Magswitch magnet.

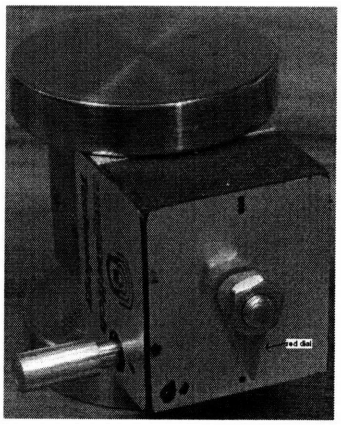

Figure 3-1: View of a Magswitch magnet

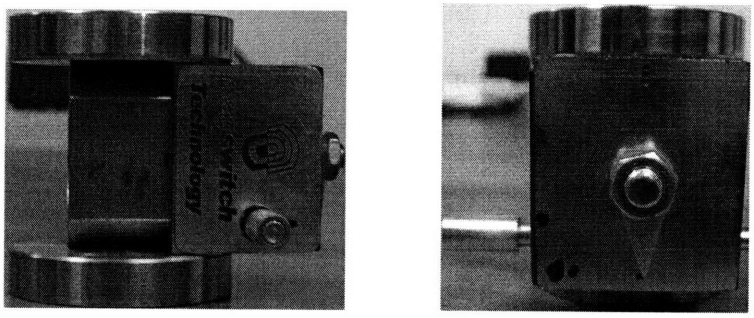

(a) Front view

(b) Side view

Figure 3-2: Front and side views of Magswitch magnet

3.2 Problems with Magswitch Magnet

One problem with the magnet is the non-uniformity of the magnetic field which causes the ferrofluid to move to the strong magnetic field region at the edges of the magnet and not remain as a round drop in the central region of the Hele-Shaw cell. Although bulky, the solenoidal magnet did produce a very uniform DC field through the Hele-Shaw cell keeping the ferrofluid drop in the center. The Magswitch magnet is smaller but produces very large fields at the edges of the magnet. This in turn pulls the ferrofluid from the center of the Hele-Shaw cell and forces it to congregate at the outer edges. In the next section, a Teslameter (Figure 2-7) will be used to accurately measure the magnetic field at different positions over the magnet as well as at different heights above the magnet. This will give a spatial distribution of the magnetic field as a function of location and height. From these measurements, the Hele-Shaw cell can be placed where the Magswitch magnet produces an approximate uniform DC field through the ferrofluid drop.

Another problem with the Magswitch magnet is the inability to access the dial once it is inside the stator winding coil. To circumvent this problem, an extension rod was built to allow easier use of the Magswitch magnet as shown in Figure 3-3.

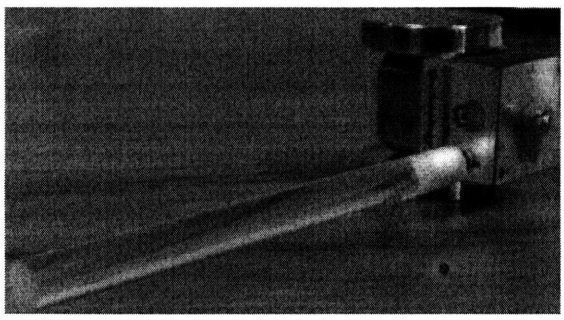

Figure 3-3: Magswitch magnet with extender on the control knob.

Once the extender is this long, the entire Magswitch magnet can no longer fit inside the stator. The inside of the stator had a diameter of 78 mm and a height of 62.5 mm. The coil had to be propped up so that the user can control the Magswitch magnet. Figure 3-4 shows a setup of the coil propped up on wooden blocks. The control knob has been extended by the large handle allowing for easier use.

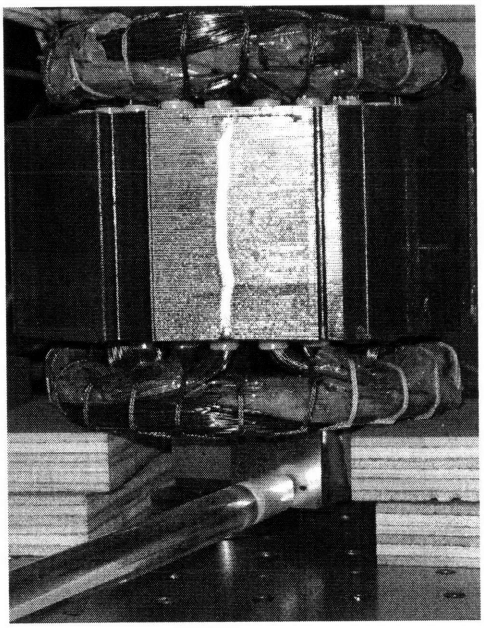

Figure 3-4: Stator winding propped on wooden blocks. Magswitch magnet with extender is placed underneath to provide DC axial field.

3.3 Magswitch Magnet Measurements in Stator

The original magnetizable top that came with the Magswitch was $\frac{3}{8}$ inches thick and had a diameter of 50 mm. This top is shown on the left in Figure 3-5. The magnetic fields at the edges of the magnet were so strong that the ferrofluid was pulled from the center of the Hele-Shaw cell to the edge. To solve this problem, a secondary magnetizable top was constructed (to the right in Figure 3-5). This secondary top was $\frac{1}{4}$ inch thick and 3 inches (76 mm) in diameter. A bigger top was built so that the outer edges would be further away from the center of the Hele-Shaw cell where the ferrofluid drop will be. This bigger top, which was 76 mm in diameter, was chosen in order to fit inside the stator which was 78 mm in diameter.

As stated, the magnetic field was measured at different positions and different heights above the Magswitch magnet when it was placed radially centered within the stator winding at a vertical height of 2 cm from the bottom of the stator winding. Figure 3-6 shows sketches of the labeling system used in this thesis. Figure 3-6(a) is a sketch for the $\frac{3}{8}$ in thick, 50 mm diameter plate. Figure 3-6(b) is a sketch for the $\frac{1}{4}$ in thick, 3 inch diameter plate. The letters

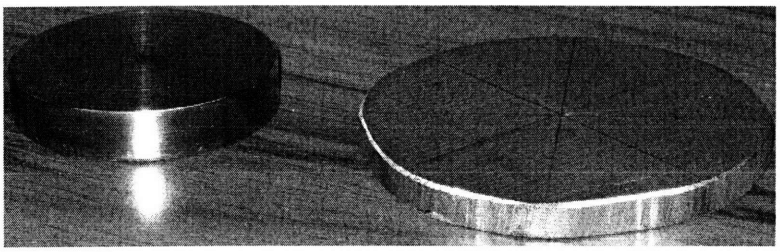

Figure 3-5: Two tops of the Magswitch magnet. The top on the left is $\frac{3}{8}$ in thick and 50 mm in diameter. The top on the right is $\frac{1}{4}$ in thick with a 3 in diameter. The larger top has a weaker magnetic field at its outer edge so that the ferrofluid drop remained in the center of the Hele-Shaw cell.

(A-Q) mark the spots in which the magnetic fields were measured. *A* marks the middle, *B-I* are on the edges 45° apart. *J-Q* are located halfway between the center and the outer edge and are also 45° apart. Letters *A,J-Q* are called the **interior** positions and *B-I* are the **exterior** positions.

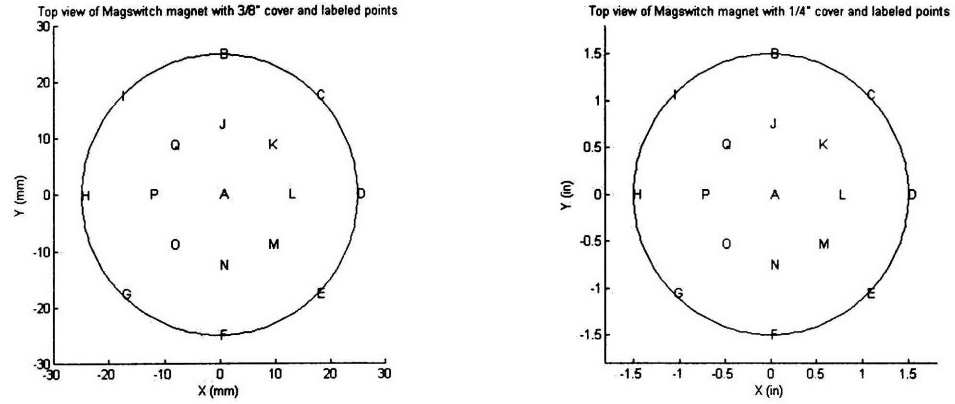

(a) (b)

Figure 3-6: Sketches of the Magswitch covers. The $\frac{3}{8}$ in thick, 50 mm diameter top is shown in (a) and the $\frac{1}{4}$ in thick, 3 in diameter top is shown in (b). The letters (A-Q) mark the spots in which the magnetic fields were measured. *A* marks the middle, *B-I* are on the edges 45° apart. *J-Q* are located halfway between the center and the outer edge and are also 45° apart. Letters *A,J-Q* are called the **interior** positions and *B-I* are the **exterior** positions.

The x, y and z components at each point was measured and are referred to as B_x, B_y, and B_z respectively. An FW Bell three axis probe (Part Number ZOA73-3208-5) was used to measure the components of the magnetic field. Figure 3-7 shows the equipment setup used

for the measurements. A microstage accurately moved up and down along the Z axis from 0 to 5 cm. A vertical rod is placed in the stage with a test tube clamp fixed to it. The clamp holds the three axis probe in place over the magnet which is inside the stator. Appendix A contains tables of the measured values of the magnetic field components of various positions using both tops.

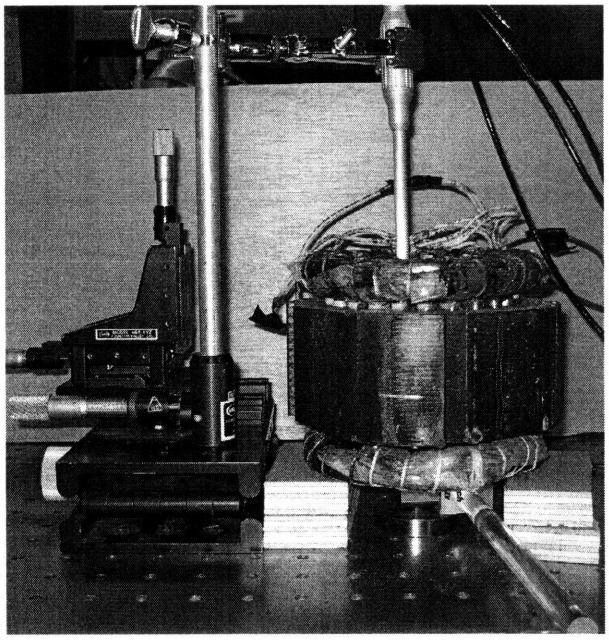

Figure 3-7: Equipment setup used to measure the DC magnetic field as a function of position on and above the Magswitch magnet. A microstage moved up and down along the z axis from 0 to 5 cm accurately. A vertical rod is placed in the stage with a test tube clamp fixed to it. The clamp holds the three axis probe in place over the magnet which is inside the stator.

3.3.1 Measurements with $\frac{3}{8}$ in thick, 50 mm diameter top

Magnetic field measurements were taken first with the original Magswitch top. This top was 50 mm in diameter and was $\frac{3}{8}$ inches thick. Table A.1 in Appendix A lists all the numerical values recorded. Figure 3-8 shows 6 plots of the normalized z, y, and z components of magnetic field magnitudes B_x,B_y and B_z. Each component was normalized by the largest magnitude which was $|B_{max}| = 840.95$ Gauss. The x axis for each plot refers to the position at which the magnetic field was measured. 1 refers to position A, 2 refers to B and so on.

Figure 3-6(a) shows a schematic of the $\frac{3}{8}$ in thick top with the positions labeled A through Q.

3.3.2 Measurements with $\frac{1}{4}$ in thick, 3 in diameter top

Subsequent magnetic field magnitude measurements were taken with the new constructed top. This top was 3 inches in diameter and was $\frac{1}{4}$ inches thick. Table A.2 in Appendix A lists all the numerical values recorded. Figure 3-8 shows 6 plots of the normalized x, y, and z components of magnetic field magnitudes B_x,B_y and B_z. Each component was normalized by the largest magnitude which was $|B_{max}| = 645.41$ Gauss. Figure 3-6(b) shows the labeling schematic of the $\frac{1}{4}$ in thick top with the positions labeled A through Q.

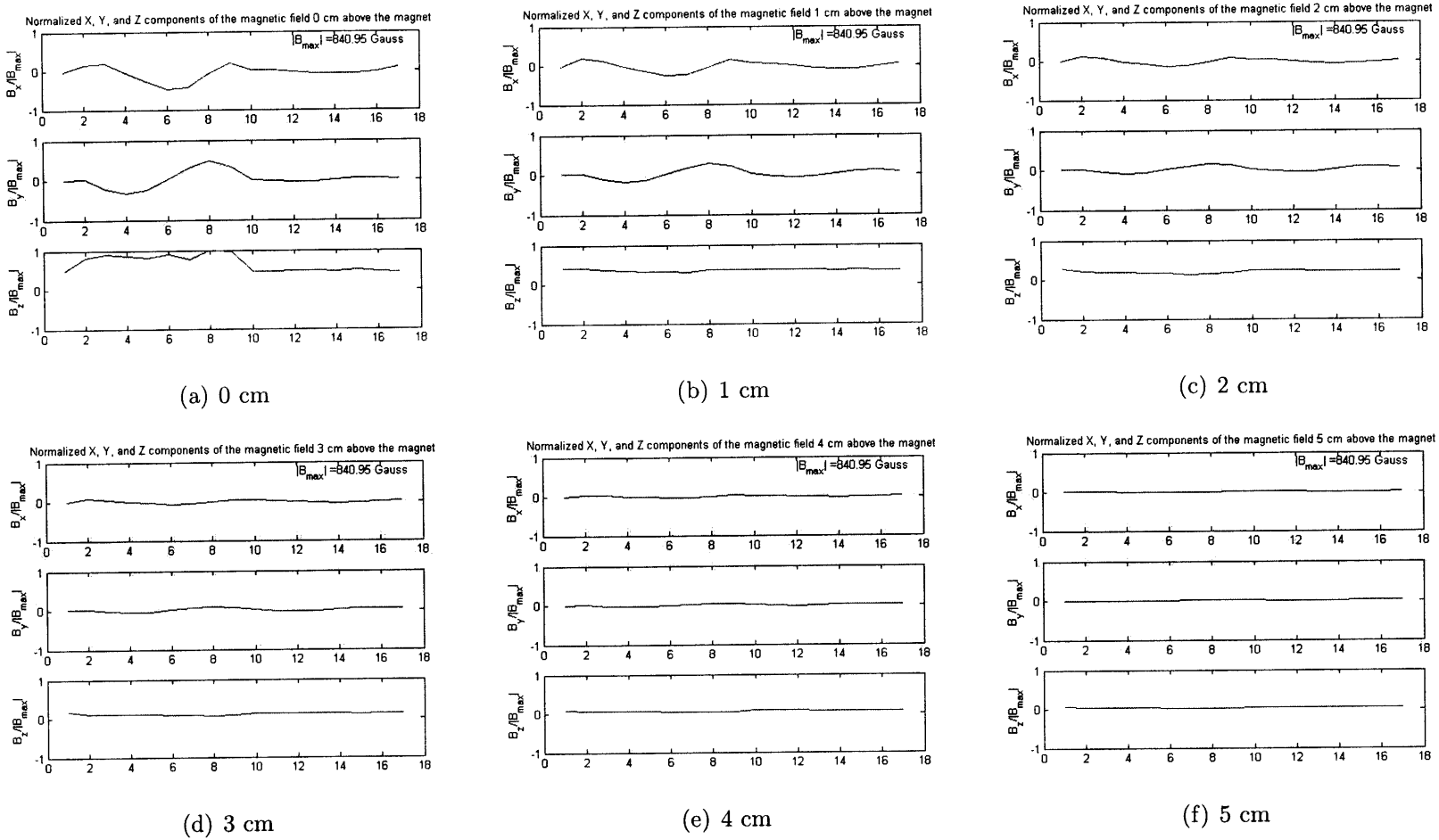

(a) 0 cm (b) 1 cm (c) 2 cm

(d) 3 cm (e) 4 cm (f) 5 cm

Figure 3-8: Normalized x, y, and z components of DC magnetic field magnitudes B_x, B_y and B_z from Table A.1 with $|B_{max}| = 840.95$ Gauss at different heights above the magnet labeled above for the $\frac{3}{8}$ in thick cover with the Magswitch magnet inside the stator. The x axis in each plot refers to position on the top of magnet as sketched in Figure 3-6(a). 1 refers to A, 2 to B and so on to 17 for Q.

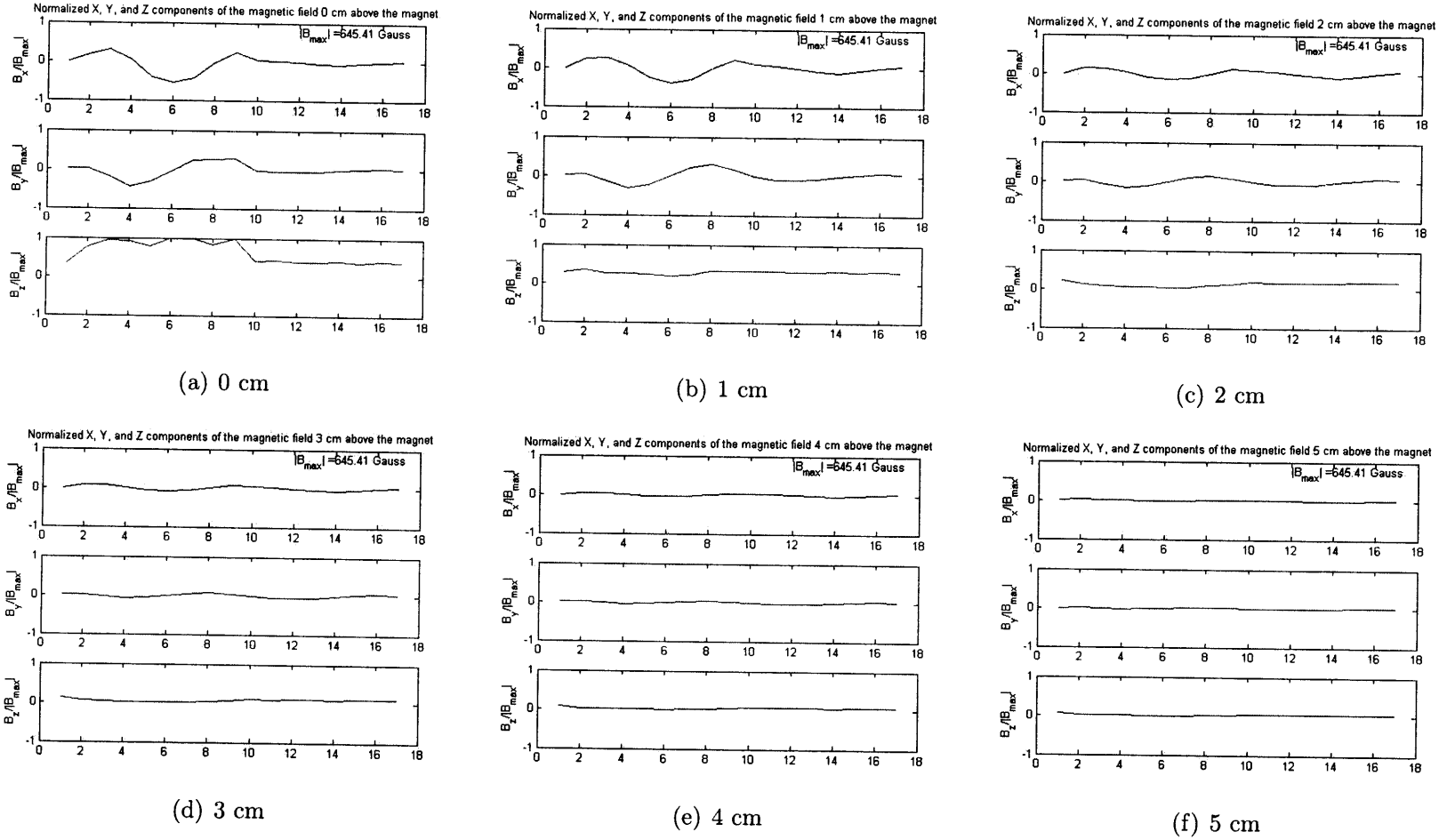

(a) 0 cm (b) 1 cm (c) 2 cm

(d) 3 cm (e) 4 cm (f) 5 cm

Figure 3-9: Normalized x, y, and z components of DC magnetic field magnitudes B_x, B_y and B_z from Table A.2 with $|B_{max}| = 645.41$ Gauss at different heights above the magnet labeled above for the $\frac{1}{4}$ in thick cover with the Magswitch maget in free space. The x axis in each plot refers to position on the top of magnet as sketched in Figure 3-6(b). 1 refers to A, 2 to B and so on to 17 for Q.

3.4 Magswitch Magnet Measurements in Free Space

In order to understand the effect of the stator winding on the magnetic field of the Magswitch magnet, measurements were also taken with the magnet in free space. Appendix B, Table B.1 lists the magnetic field components, as a function of position and height, for the magnet with the constructed 3 inch, $\frac{3}{8}$ inch top in free space with the stator removed. Table B.2 contains the magnetic field components for the original 50 mm, $\frac{1}{4}$ in thick top.

Figure 3-10 graphically compares the three components of the magnetic field of the Magswitch magnet inside the stator and in free space asa function of z, the height above the Magswitch magnet. The interior and exterior points are defined in Figure 3-6. The measurements taken with the magnet inside the stator are plotted with solid lines while those taken in free space are plotted with dashed lines. As shown in (e) and (f) the B_z component of the magnetic field is smaller in amplitude when the magnet is placed in the stator than when it is in free space. As expected, the iron inside the stator forces the magnetic field lines to bend and terminate onto the iron. This reduces the strength of the magnetic field in the z direction.

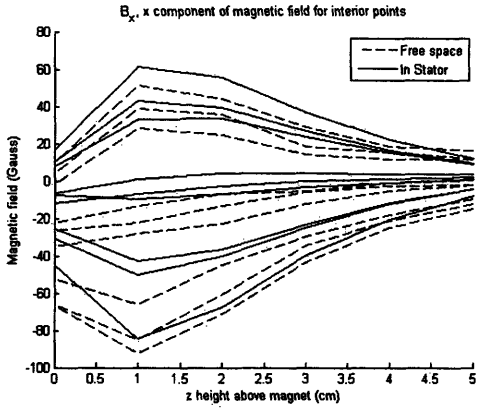

(a) B_x for interior points.

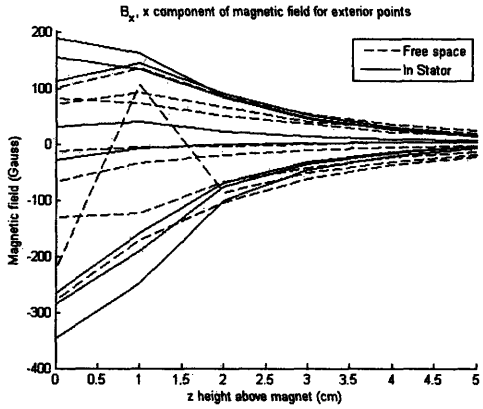

(b) B_x for exterior points.

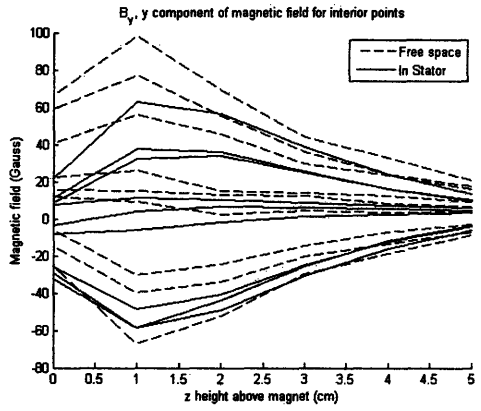

(c) B_y for interior points.

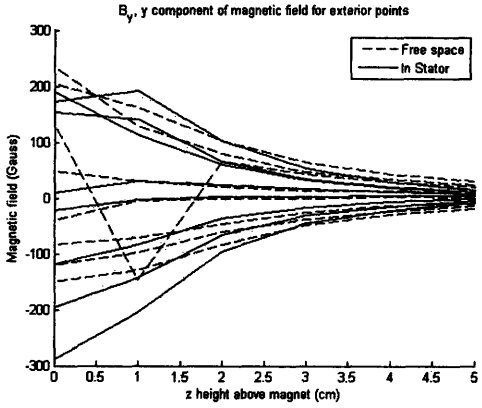

(d) B_y for exterior points.

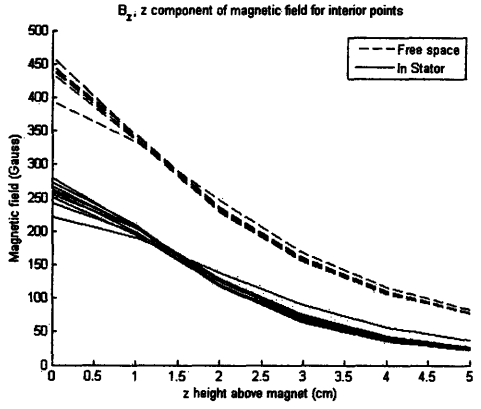

(e) B_z for interior points.

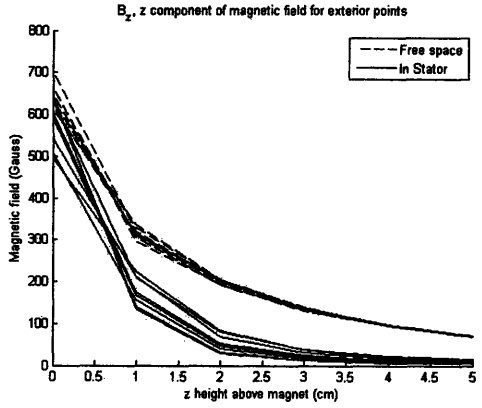

(f) B_z for exterior points.

Figure 3-10: Comparison of the three components of the DC magnetic field of the Magswitch magnet inside the stator and in free space. The x axis is z, the height above the magnet. The interior and exterior points are defined in Figure 3-6. The measurements taken with the magnet inside the stator are plotted with solid lines while those taken in free space are plotted with dashed lines.

3.5 Discussion

The Magswitch magnet was used as a way to provide a controllable DC axial field. Compact in size, the magnet also does not require power and is therefore a viable portable option to previous equipment. One negative aspect to the Magswitch magnet is its non-uniform magnetic field. A new constructed top with a 3 inch diameter was built so that the large fringing fields at the ends of the top are farther away from the center where the ferrofluid drop will be. This allows the ferrofluid drop to remain in the center of the Hele-Shaw cell.

B_z, the z component of the magnetic field, is an important measurement since this is the axial field for the Hele-Shaw cell. This component needs to be strong enough to produce the labyrinth and phase transition patterns seen in previous experiments described in Chapter 2. In those experiments, a DC field of about 80 Gauss produced the labyrinth pattern and a DC field on the order of 140 Gauss produced the phase transitions. Table A.2 shows that a height between 2 and 3 cm above the magnet had a magnetic field with its z component in this range.

The x and y components of the magnetic field are also important in that they pull the ferrofluid drop away from the center of the Hele-Shaw cell. This undesirable result can be reduced if a height is selected so that these components are as uniform as possible. Figure 3-9 shows the three components of the magnetic field at different positions on top of the magnet at different heights. The first two graphs in each plot are the x and y components, respectively. At 5 cm above the magnet (Figure 3-9(f)), these components look most uniform. However, the z component of the magnetic field becomes too weak to create the patterns needed. Between 2 cm (Figure 3-9(c)) and 3 cm (Figure 3-9(d)), the x component is not perfectly uniform but is more uniform at 3 cm. There needs to be a trade-off between uniformity of the x and y components while still having a strong enough z component. The final choice was to put the Hele-Shaw cell at 2.5 cm, midway between 2 and 3 cm.

To place the Hele Shaw cell 2.5 cm above the magnet, nonmagnetic plastic spacers were placed on top of the Magswitch magnet. Figure 3-11 shows a picture of the setup.

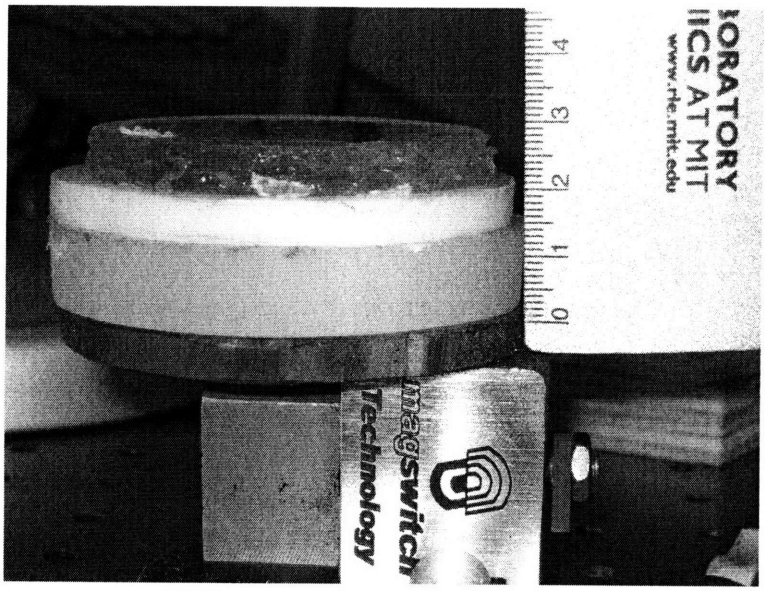

Figure 3-11: View of nonmagnetic nonmagnetic plastic spacers placed on the top of the Magswitch magnet. The ferrofluid drop in the Hele-Shaw cell is now 2.5 cm from the top of the Magswitch magnet.

Chapter 4

Results

In this section, the images are shown for the labyrinth spirals and the phase transitions. The following images were obtained using the Magswitch magnet to provide the axial DC magnetic field. The Hele-Shaw cell was also placed 2.5 cm over the magnet as shown in Figure 3-11.

4.1 Labyrinth Spirals

Figures 4-1 to 4-9 show the labyrinth spiral patterns. The Magswitch magnet magnetic field is set to the value stated in the corresponding figure's caption for various values of rotating magnetic field amplitude and frequency.

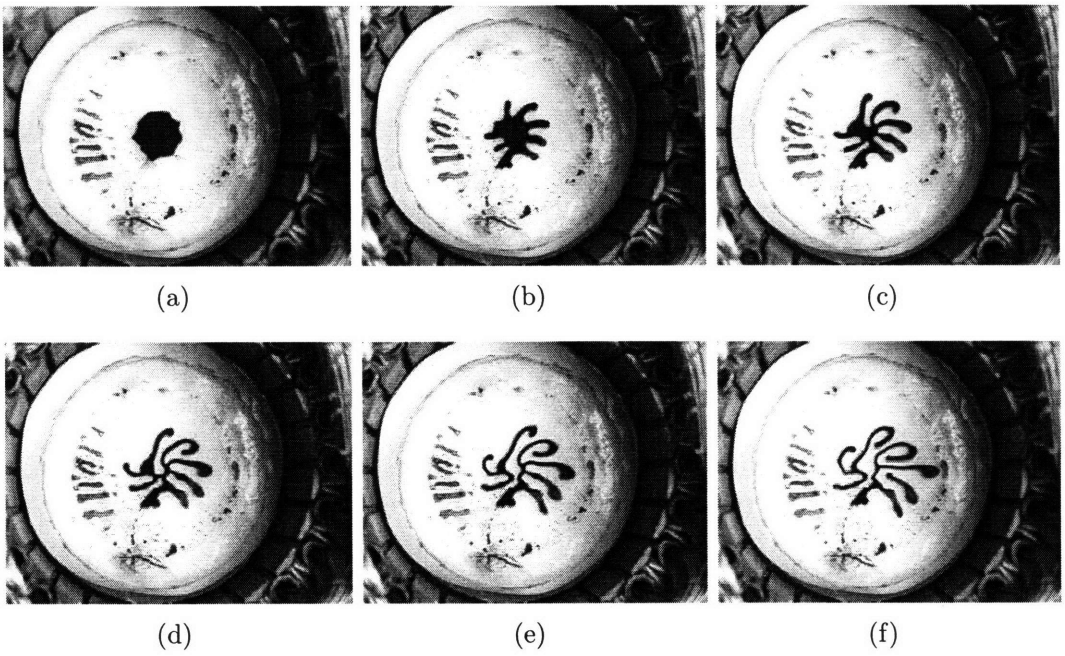

Figure 4-1: Sequence of labyrinth patterns. Magswitch magnet produces a 71.3 Gauss axial DC magnetic field. The stator coil winding is excited to produce a 15 Hz, 30.0 Gauss CW rotating magnetic field.

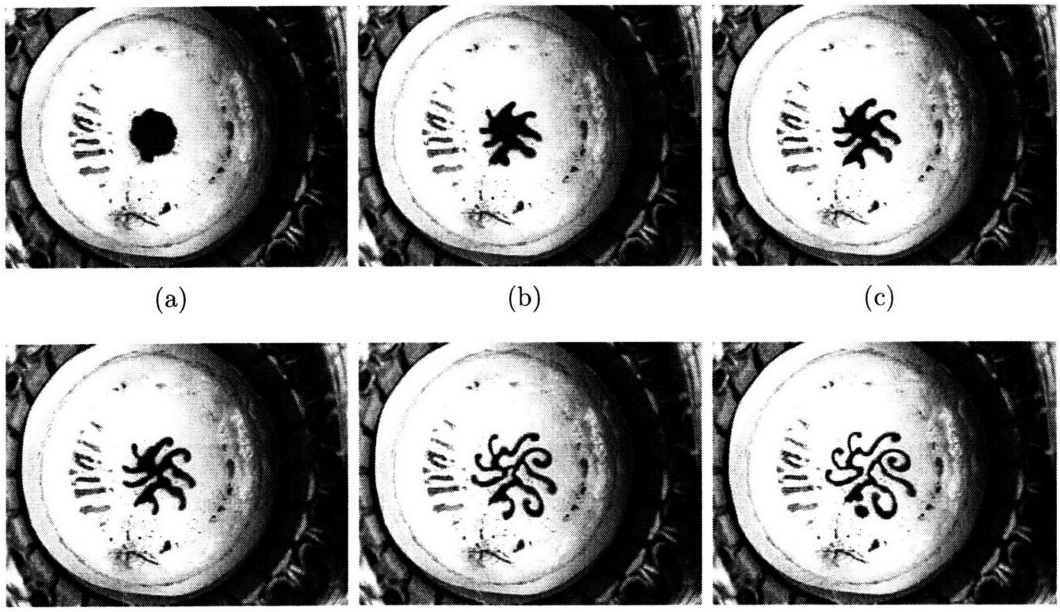

Figure 4-2: Sequence of labyrinth patterns. Magswitch magnet produces a 71.3 Gauss axial DC magnetic field. The stator coil winding is excited to produce a 15 Hz, 32.9 Gauss CW rotating magnetic field.

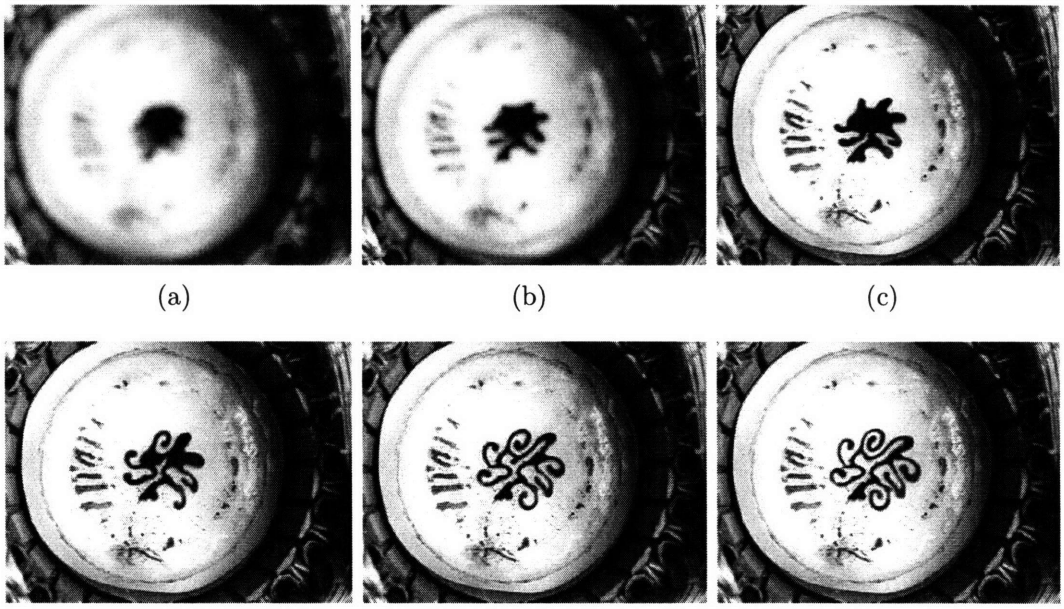

(a) (b) (c)

(d) (e) (f)

Figure 4-3: Sequence of labyrinth patterns. Magswitch magnet produces a 71.3 Gauss axial DC magnetic field. The stator coil winding is excited to produce a 15 Hz, 36.4 Gauss CW rotating magnetic field.

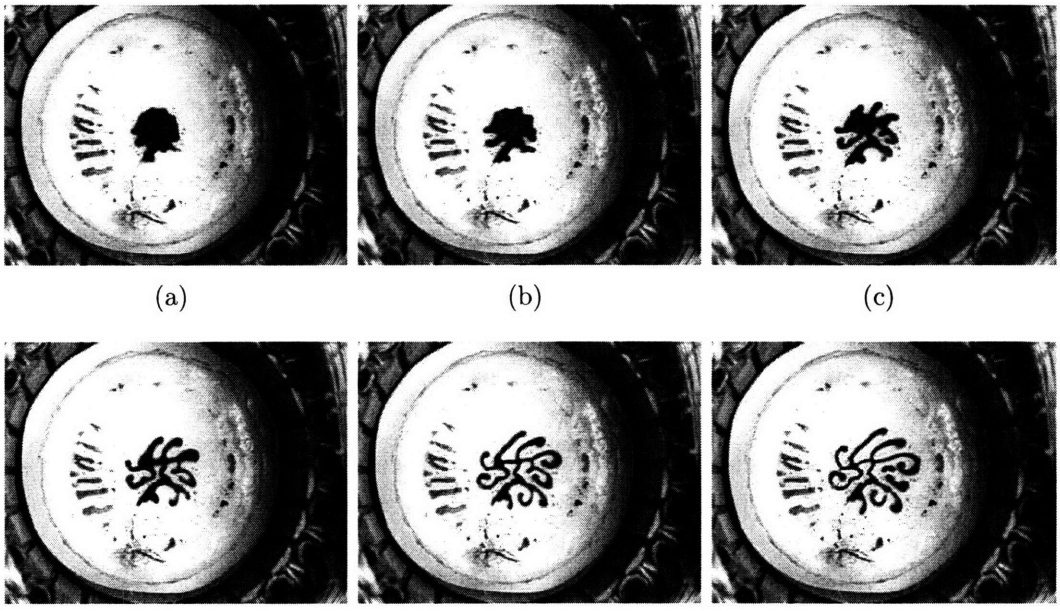

(a) (b) (c)

(d) (e) (f)

Figure 4-4: Sequence of labyrinth patterns. Magswitch magnet produces a 71.2 Gauss axial DC magnetic field. The stator coil winding is excited to produce a 20 Hz, 31.2 Gauss CW rotating magnetic field.

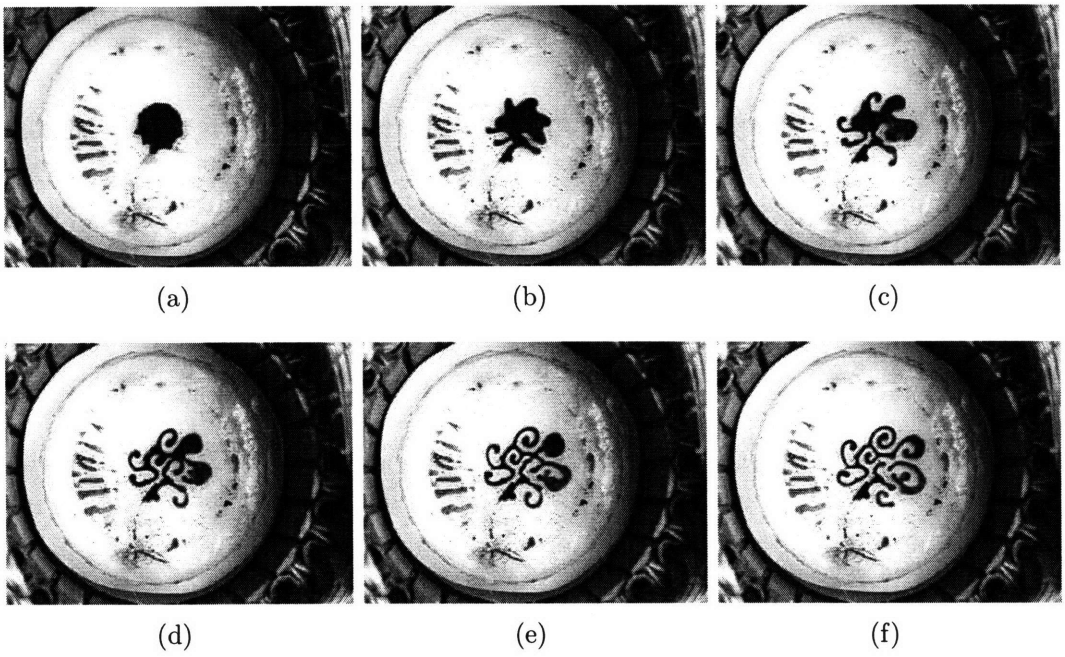

Figure 4-5: Sequence of labyrinth patterns. Magswitch magnet produces a 73.4 Gauss axial DC magnetic field. The stator coil winding is excited to produce a 20 Hz, 33.8 Gauss CW rotating magnetic field.

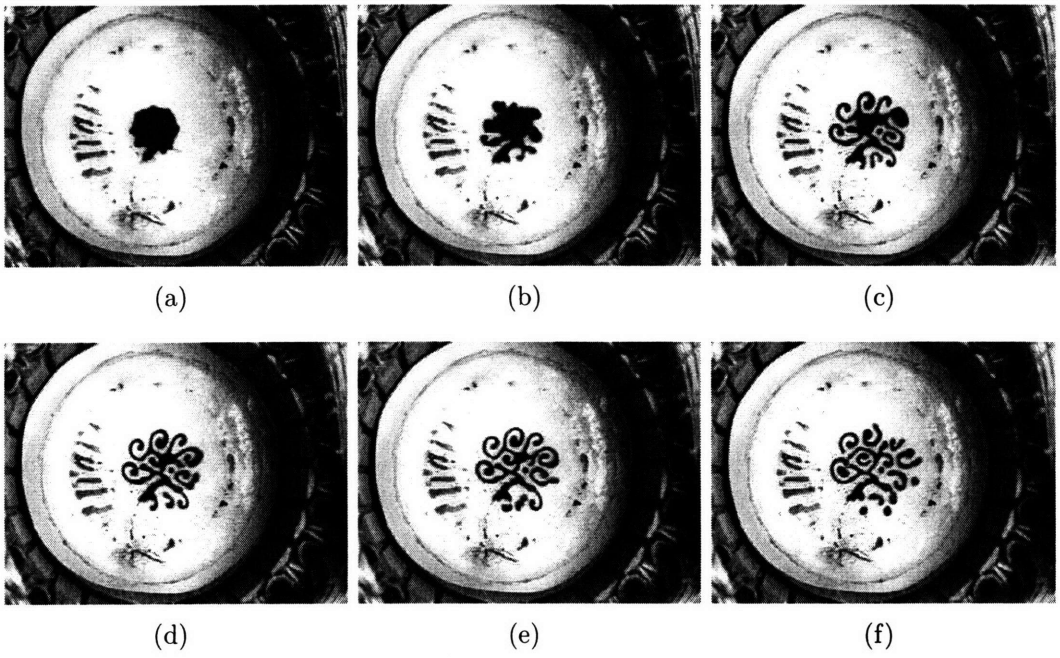

(a) (b) (c)

(d) (e) (f)

Figure 4-6: Sequence of labyrinth patterns. Magswitch magnet produces a 77.5 Gauss axial DC magnetic field. The stator coil winding is excited to produce a 20 Hz, 40.6 Gauss CW rotating magnetic field.

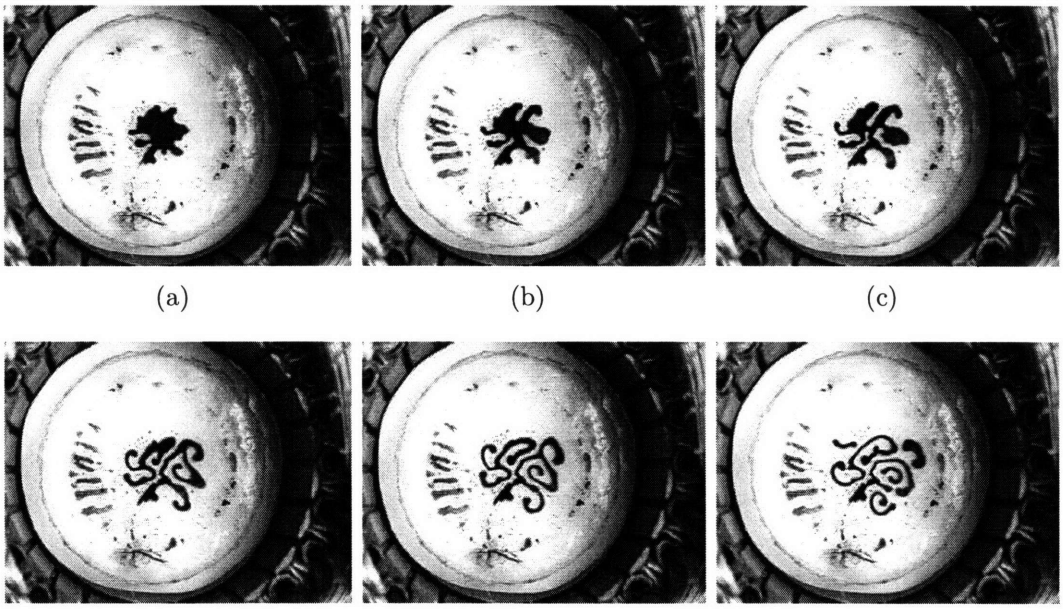

Figure 4-7: Sequence of labyrinth patterns. Magswitch magnet produces a 71.8 Gauss axial DC magnetic field. The stator coil winding is excited to produce a 25 Hz, 28.1 Gauss CW rotating magnetic field.

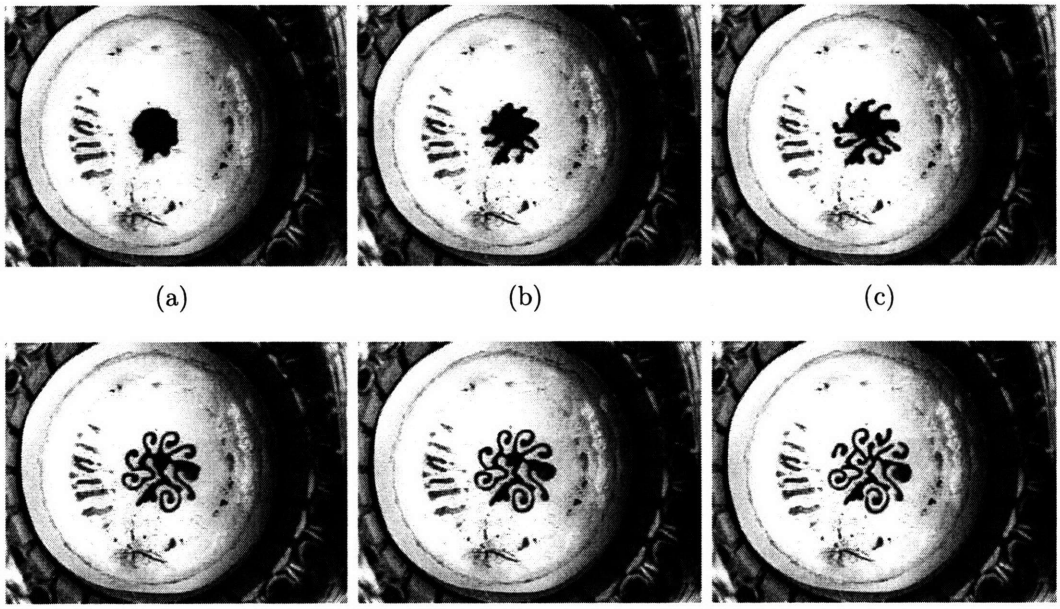

Figure 4-8: Sequence of labyrinth patterns. Magswitch magnet produces a 77.5 Gauss axial DC magnetic field. The stator coil winding is excited to produce a 25 Hz, 33.9 Gauss CW rotating magnetic field.

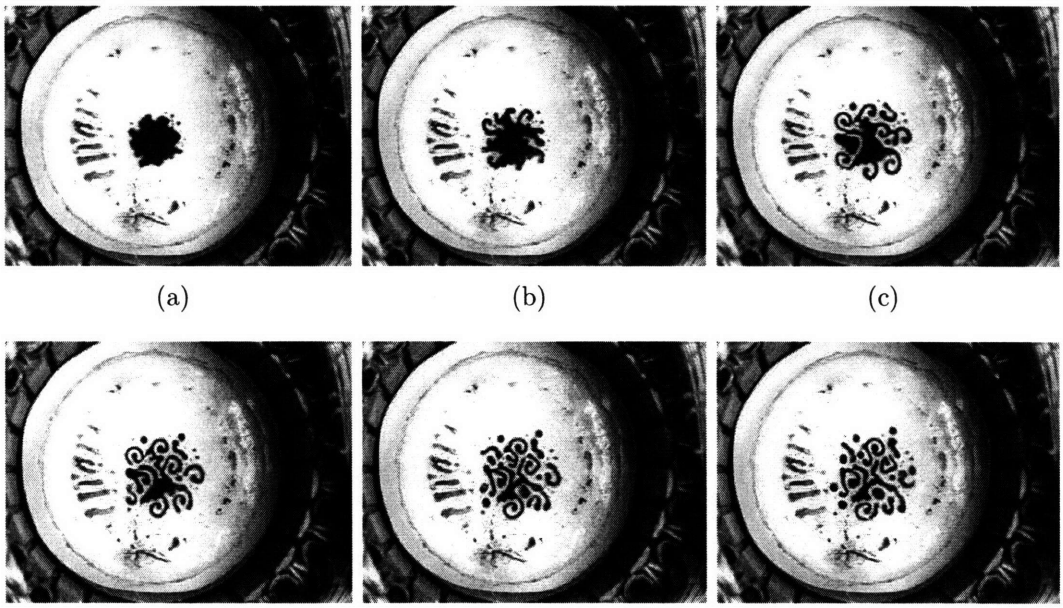

(a) (b) (c)

(d) (e) (f)

Figure 4-9: Sequence of labyrinth patterns. Magswitch magnet produces a 83.2 Gauss axial DC magnetic field. The stator coil winding is excited to produce a 25 Hz, 40.9 Gauss CW rotating magnetic field.

4.2 Phase Transitions

Figures 4-10 to 4-18 show the phase transition patterns for various values of rotating magnetic field amplitude and frequency. The Magswitch magnet magnetic field is slowly increased to the value stated in the corresponding figure's caption.

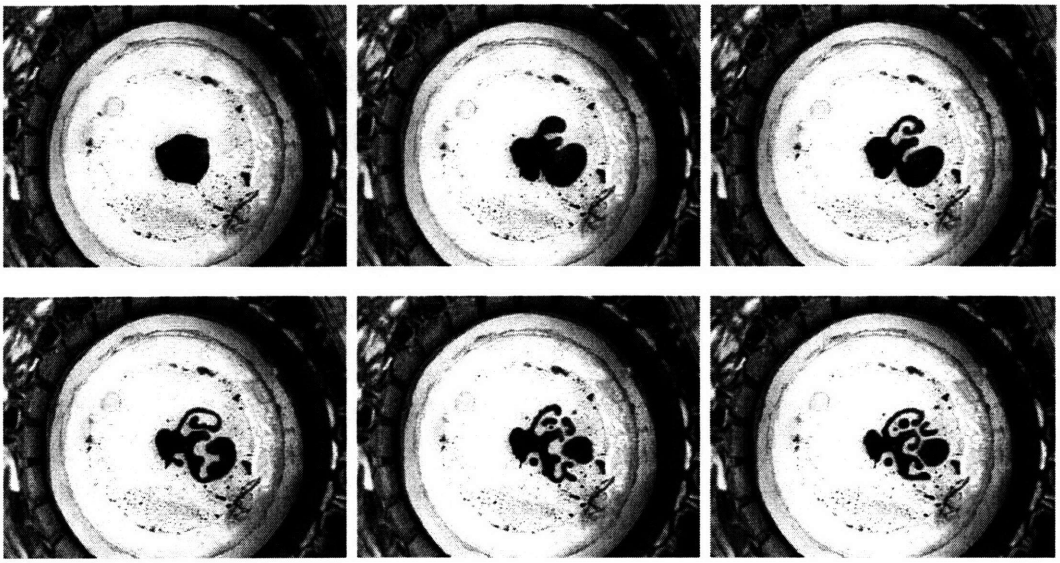

Figure 4-10: Sequence of phase transition patterns. The stator coil winding is excited to produce a 25 Hz, 31.4 Gauss CW rotating magnetic field. The Magswitch magnet is slowly increased to a final value of 66.5 Gauss to provide the axial DC magnetic field.

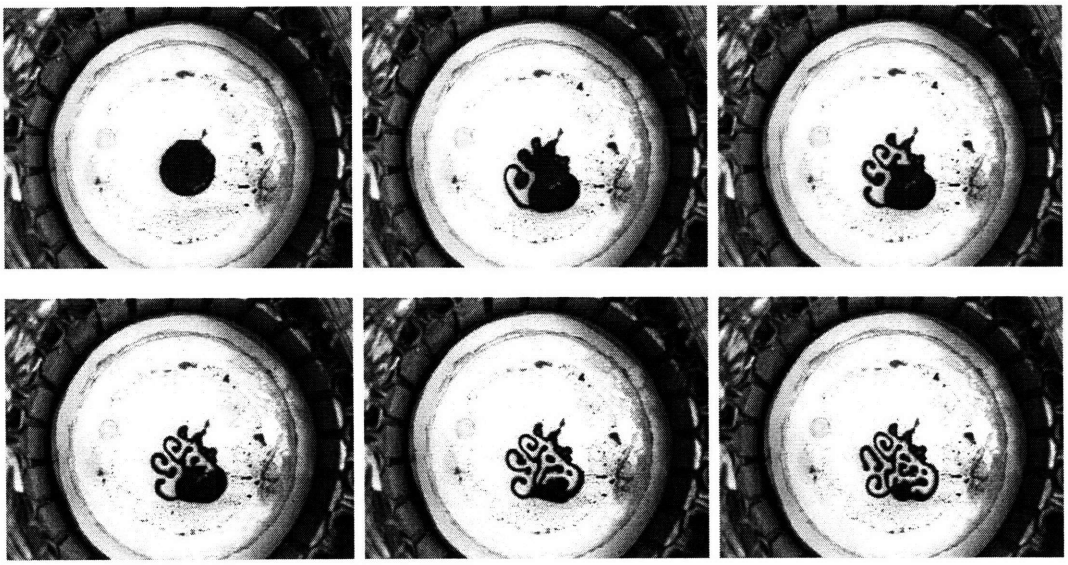

Figure 4-11: Sequence of phase transition patterns. The stator coil winding is excited to produce a 25 Hz, 33.92 Gauss CW rotating magnetic field. The Magswitch magnet is slowly increased to a final value of 79.9 Gauss to provide the axial DC magnetic field.

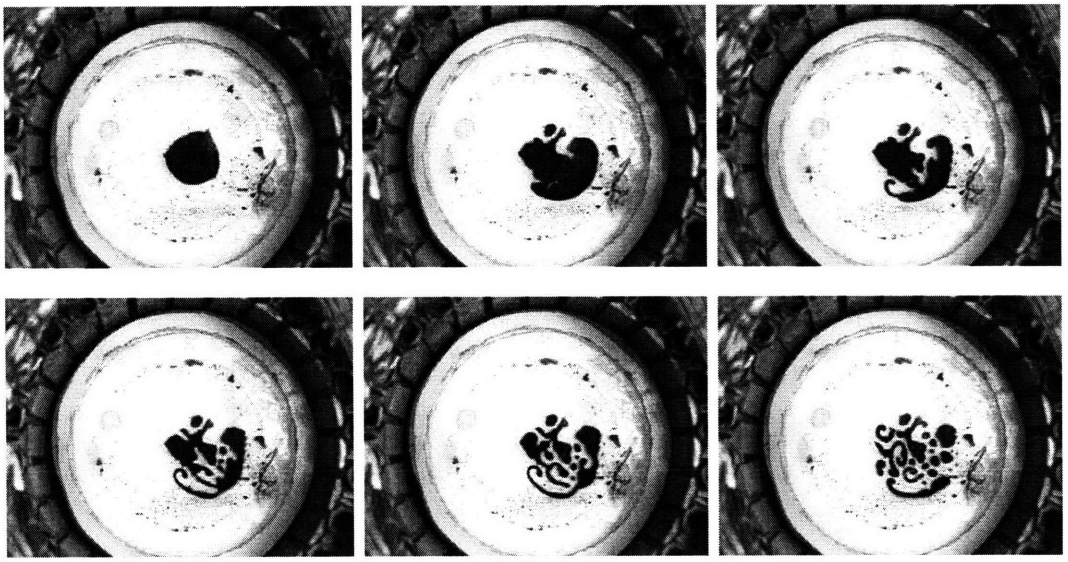

Figure 4-12: Sequence of phase transition patterns. The stator coil winding is excited to produce a 25 Hz, 40.2 Gauss CW rotating magnetic field. The Magswitch magnet is slowly increased to a final value of 74.5 Gauss to provide the axial DC magnetic field.

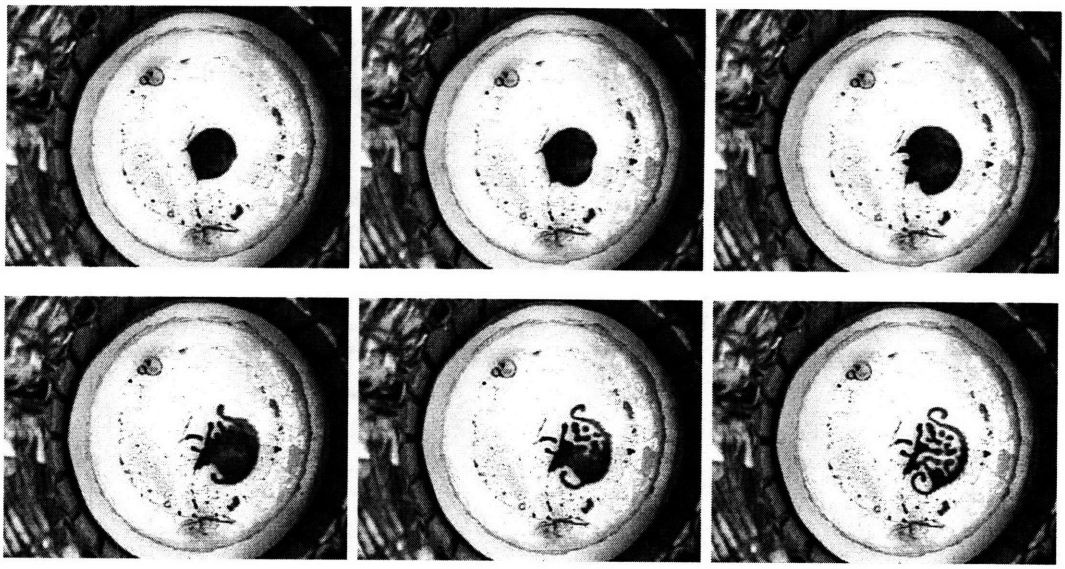

Figure 4-13: Sequence of phase transition patterns. The stator coil winding is excited to produce a 30 Hz, 31.16 Gauss CW rotating magnetic field. The Magswitch magnet is slowly increased to a final value of 77.57 Gauss to provide the axial DC magnetic field.

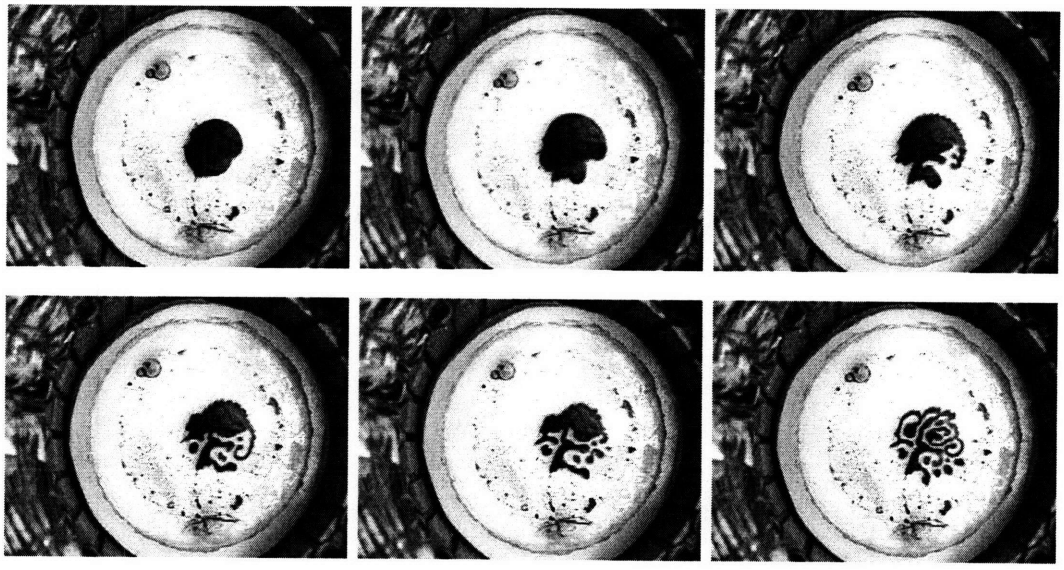

Figure 4-14: Sequence of phase transition patterns. The stator coil winding is excited to produce a 30 Hz, 35.1 Gauss CW rotating magnetic field. The Magswitch magnet is slowly increased to a final value of 77.17 Gauss to provide the axial DC magnetic field.

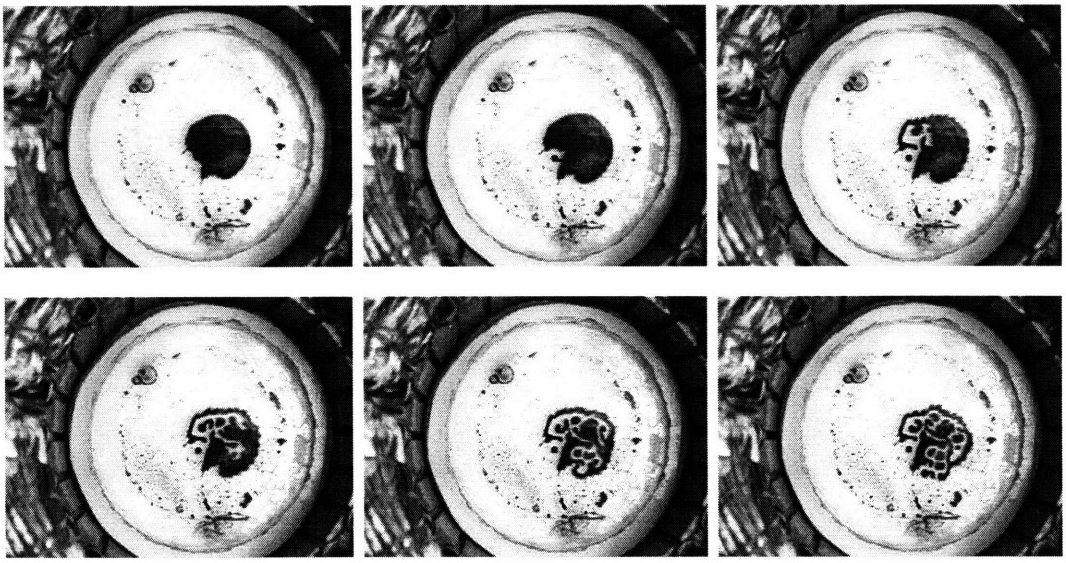

Figure 4-15: Sequence of phase transition patterns. The stator coil winding is excited to produce a 30 Hz, 37.4 Gauss CW rotating magnetic field. The Magswitch magnet is slowly increased to a final value of 84.9 Gauss to provide the axial DC magnetic field.

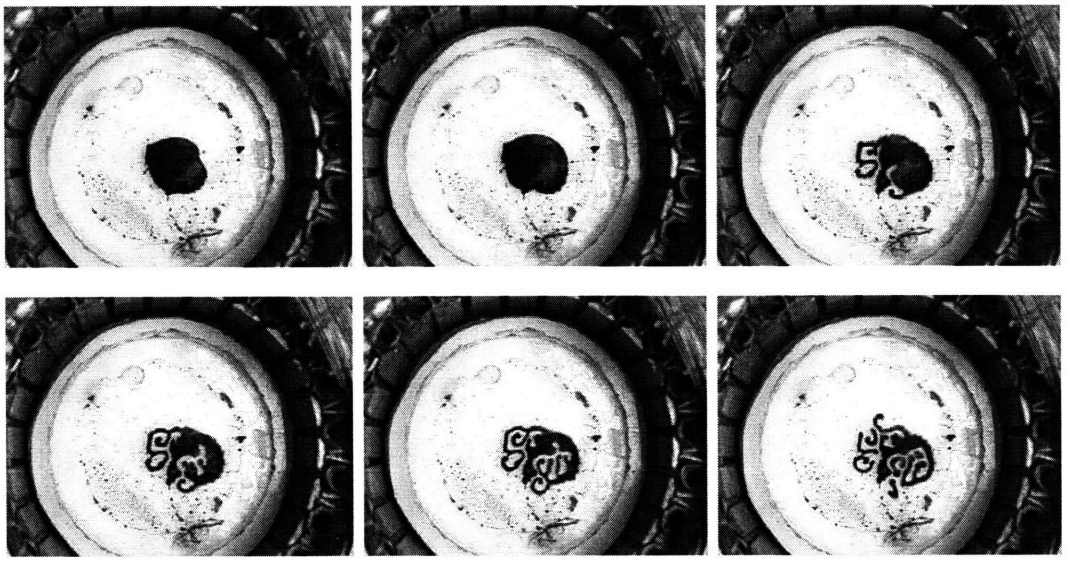

Figure 4-16: Sequence of phase transition patterns. The stator coil winding is excited to produce a 35 Hz, 31.6 Gauss CW rotating magnetic field. The Magswitch magnet is slowly increased to a final value of 84.8 Gauss to provide the axial DC magnetic field.

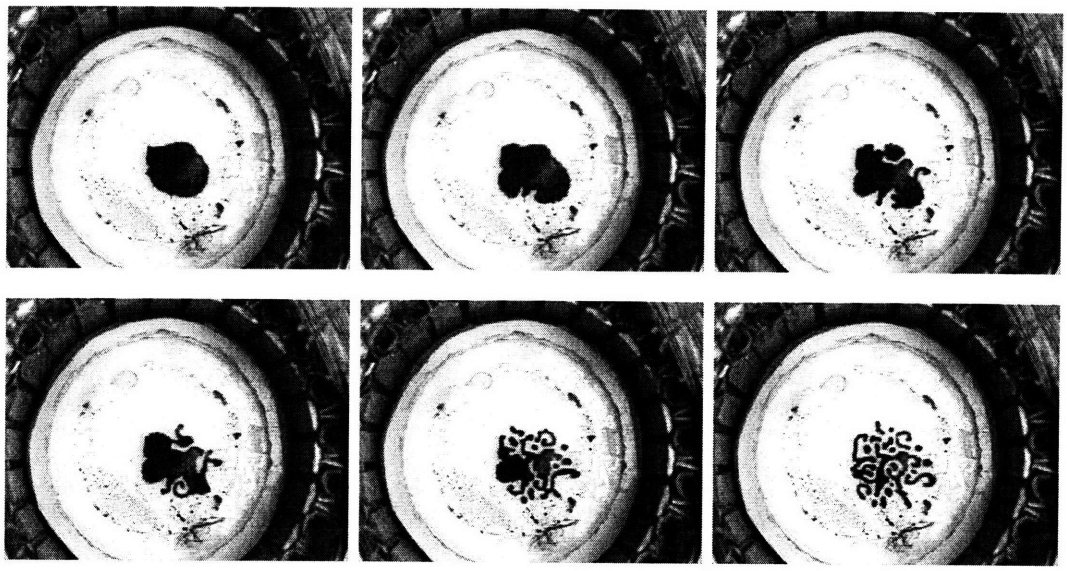

Figure 4-17: Sequence of phase transition patterns. The stator coil winding is excited to produce a 35 Hz, 34.5 Gauss CW rotating magnetic field. The Magswitch magnet is slowly increased to a final value of 85.9 Gauss to provide the axial DC magnetic field.

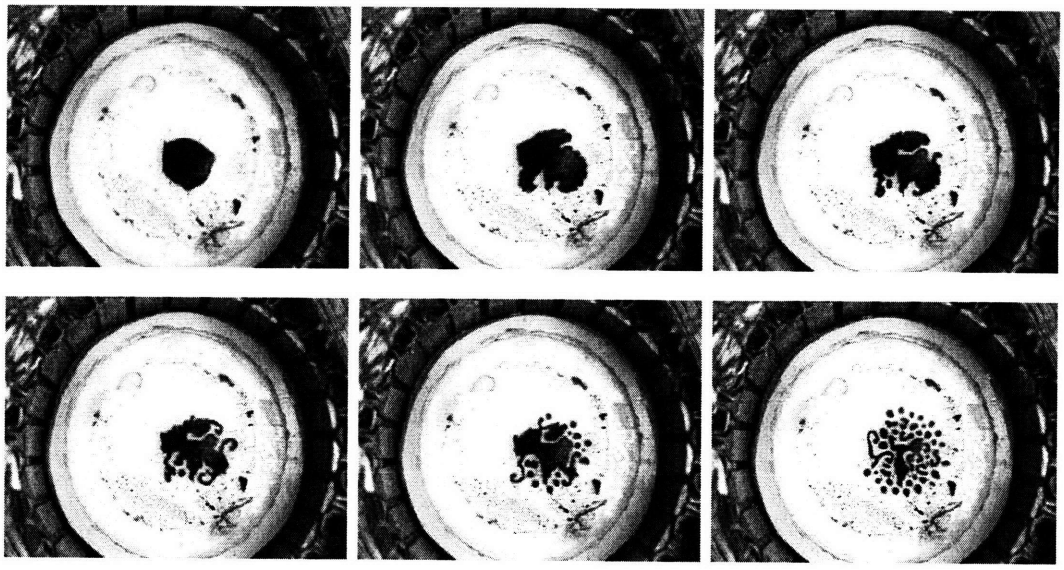

Figure 4-18: Sequence of phase transition patterns. The stator coil winding is excited to produce a 35 Hz, 39.1 Gauss CW rotating magnetic field. The Magswitch magnet is slowly increased to a final value of 89.7 Gauss to provide the axial DC magnetic field.

4.3 Phase Transitions With Permanent Magnet

THe Magswitch magnet did not produce the elaborate patterns that were as good as those shown in Sections 2.3.1 and 2.3.2. A permanent magnet was used to replace the Magswitch magnet. This permanent magnet was 1 inch in diameter with a $\frac{1}{4}$ inch thickness. Using a Gaussmeter probe, the measured z component magnetic field was -3134.1 Gauss at the center of the magnet and directly on its surface. The magnet was slowly moved toward the Hele-Shaw cell until the phase transition patterns appears. This critical distance, the distance from the Hele-Shaw cell, is recorded in the caption of the following figures.

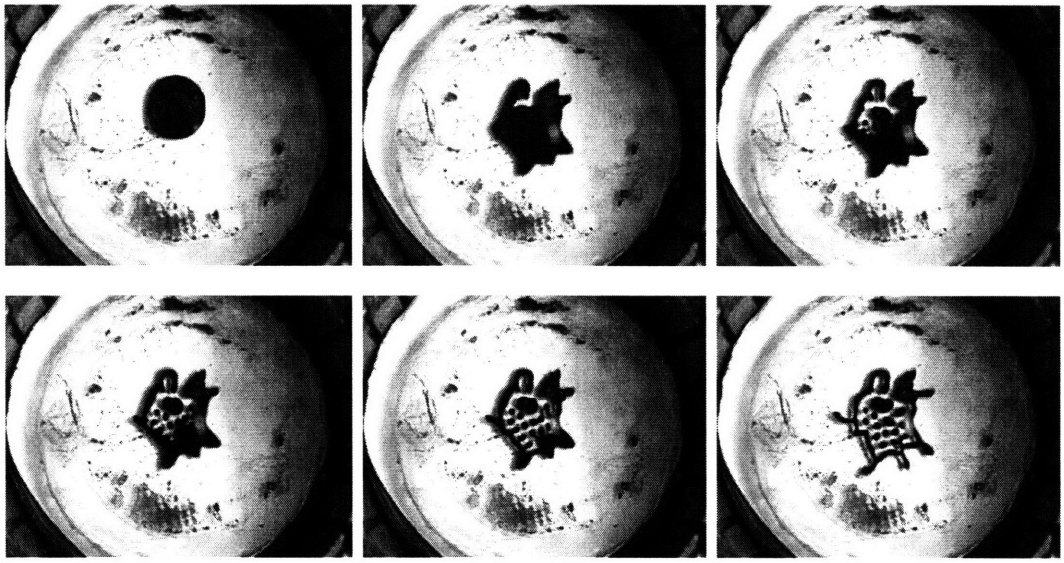

Figure 4-19: Sequence of phase transition patterns. The stator coil winding is excited to produce a 25 Hz, 18.3 Gauss CW rotating magnetic field. The 3134 Gauss permanent magnet is slowly brought toward the Hele-Shaw cell to a final critical distance of 4.3 cm to provide the axial DC magnetic field.

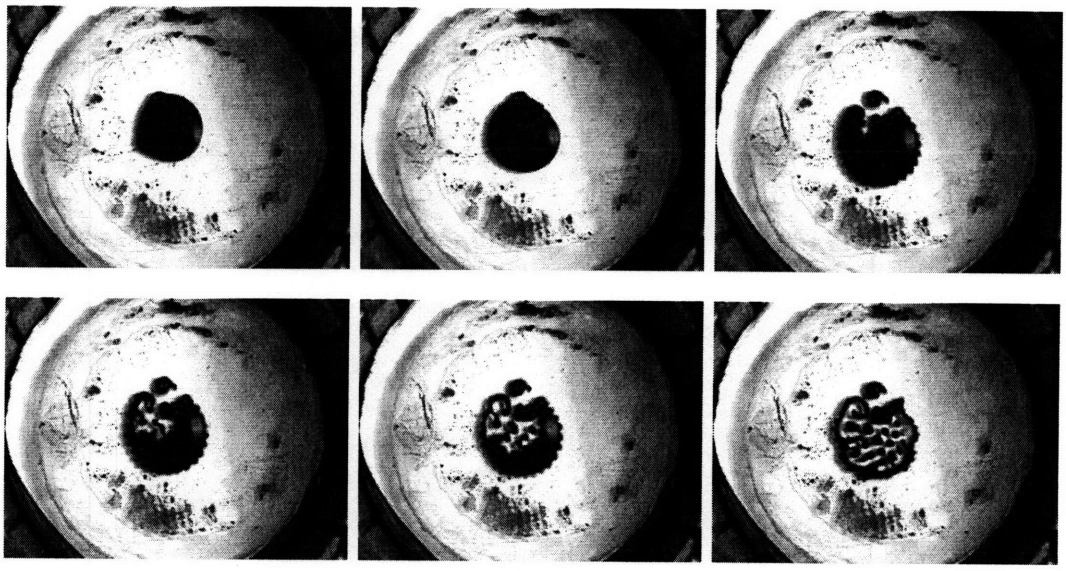

Figure 4-20: Sequence of phase transition patterns. The stator coil winding is excited to produce a 25 Hz, 25.3 Gauss CW rotating magnetic field. The 3134 Gauss permanent magnet is slowly brought toward the Hele-Shaw cell to a final critical distance of 4.4 cm to provide the axial DC magnetic field.

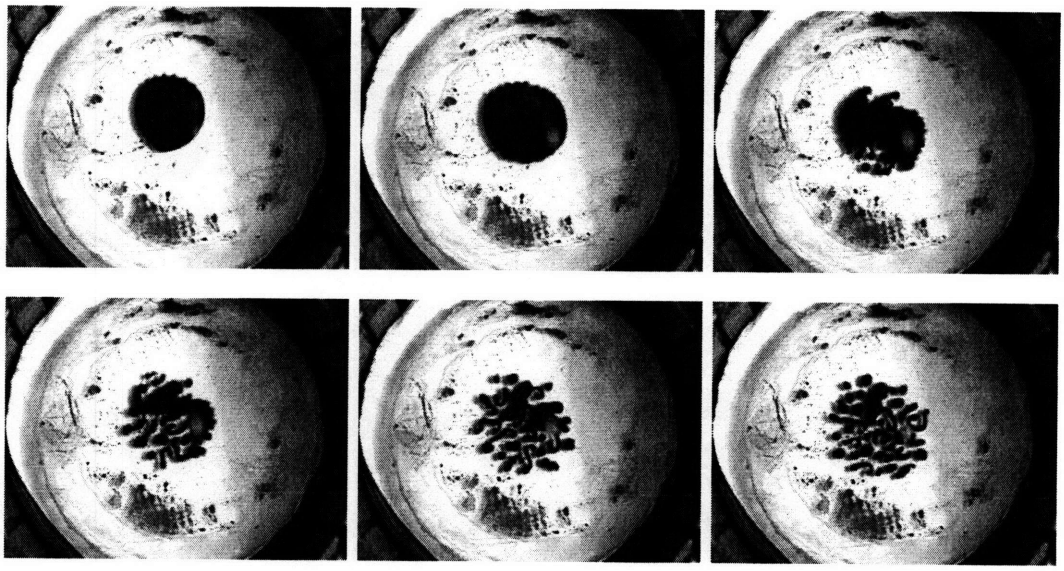

Figure 4-21: Sequence of phase transition patterns. The stator coil winding is excited to produce a 25 Hz, 30.3 Gauss CW rotating magnetic field. The 3134 Gauss permanent magnet is slowly brought toward the Hele-Shaw cell to a final critical distance of 4.4 cm to provide the axial DC magnetic field.

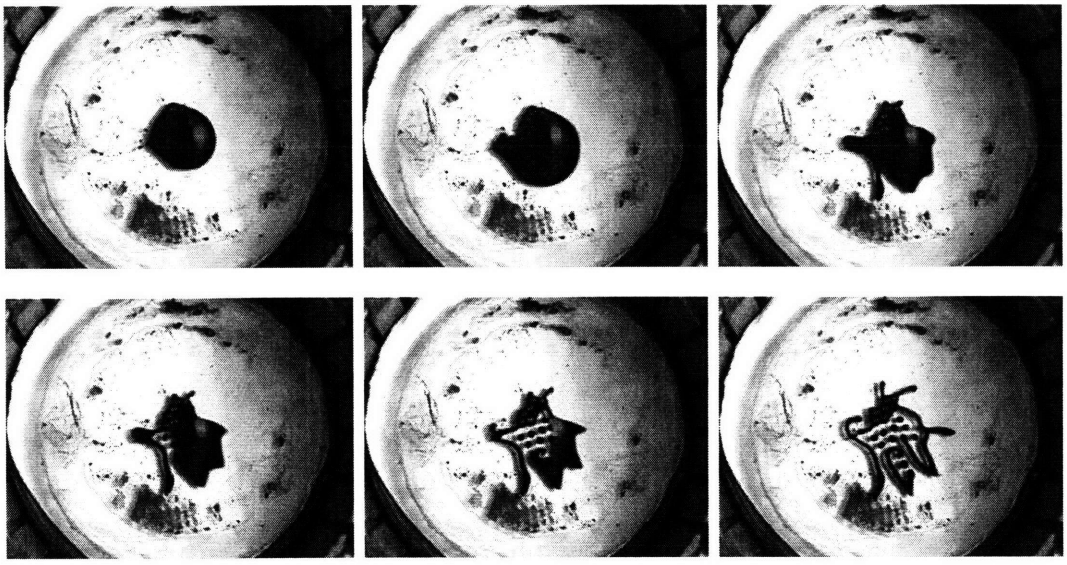

Figure 4-22: Sequence of phase transition patterns. The stator coil winding is excited to produce a 30 Hz, 17.8 Gauss CW rotating magnetic field. The 3134 Gauss permanent magnet is slowly brought toward the Hele-Shaw cell to a final critical distance of 4.3 cm to provide the axial DC magnetic field.

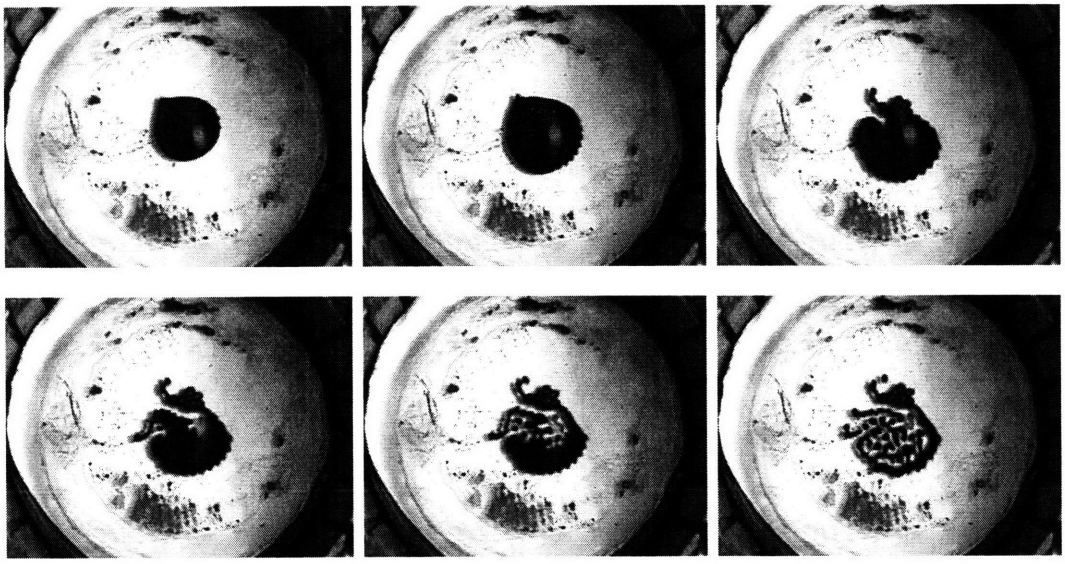

Figure 4-23: Sequence of phase transition patterns. The stator coil winding is excited to produce a 30 Hz, 25.5 Gauss CW rotating magnetic field. The permanent magnet is slowly brought toward the Hele-Shaw cell to a final critical distance of 4.4 cm to provide the axial DC magnetic field.

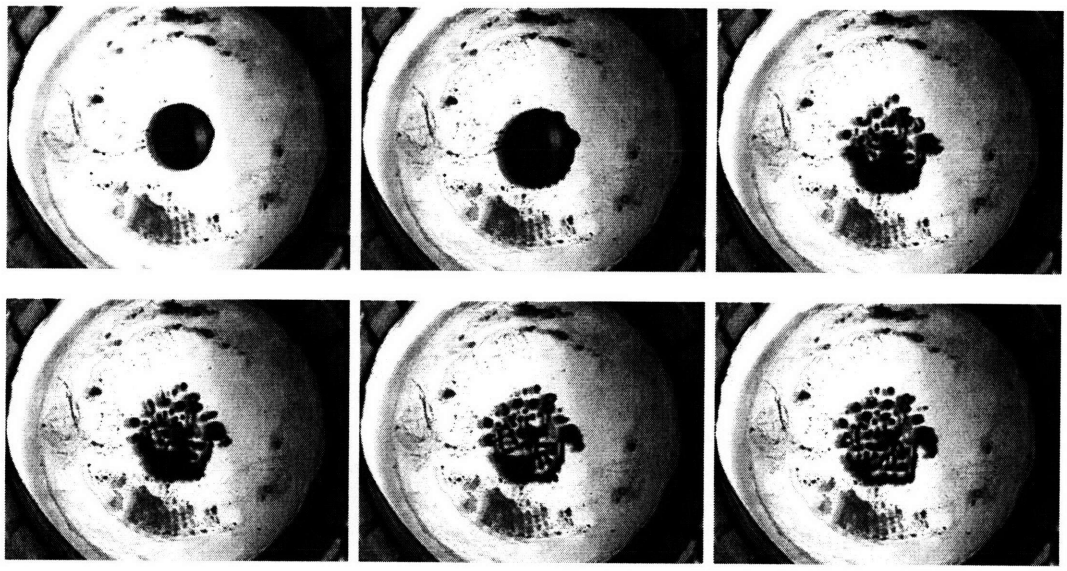

Figure 4-24: Sequence of phase transition patterns. The stator coil winding is excited to produce a 30 Hz, 30.6 Gauss CW rotating magnetic field. The 3134 Gauss permanent magnet is slowly brought toward the Hele-Shaw cell to a final critical distance of 4.3 cm to provide the axial DC magnetic field.

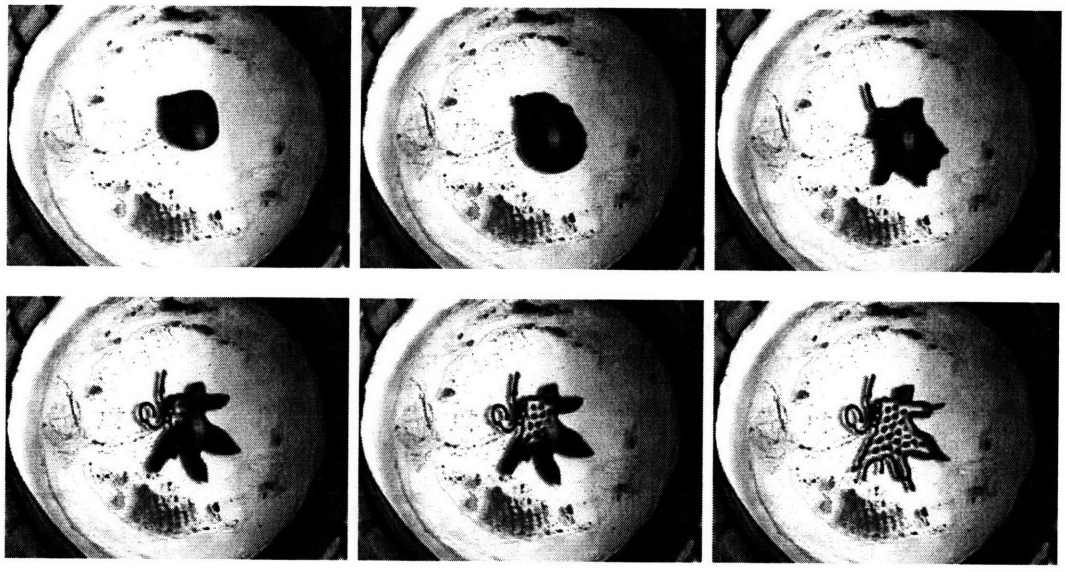

Figure 4-25: Sequence of phase transition patterns. The stator coil winding is excited to produce a 35 Hz, 18.6 Gauss CW rotating magnetic field. The 3134 Gauss permanent magnet is slowly brought toward the Hele-Shaw cell to a final critical distance of 3.9 cm to provide the axial DC magnetic field.

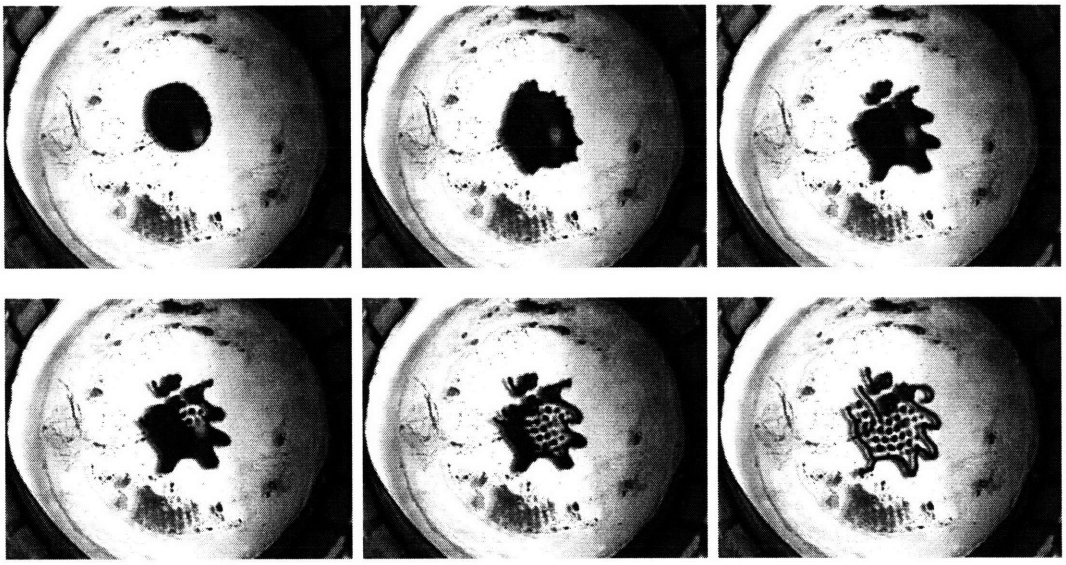

Figure 4-26: Sequence of phase transition patterns. The stator coil winding is excited to produce a 35 Hz, 25.9 Gauss CW rotating magnetic field. The 3134 Gauss permanent magnet is slowly brought toward the Hele-Shaw cell to a final critical distance of 4.1 cm to provide the axial DC magnetic field.

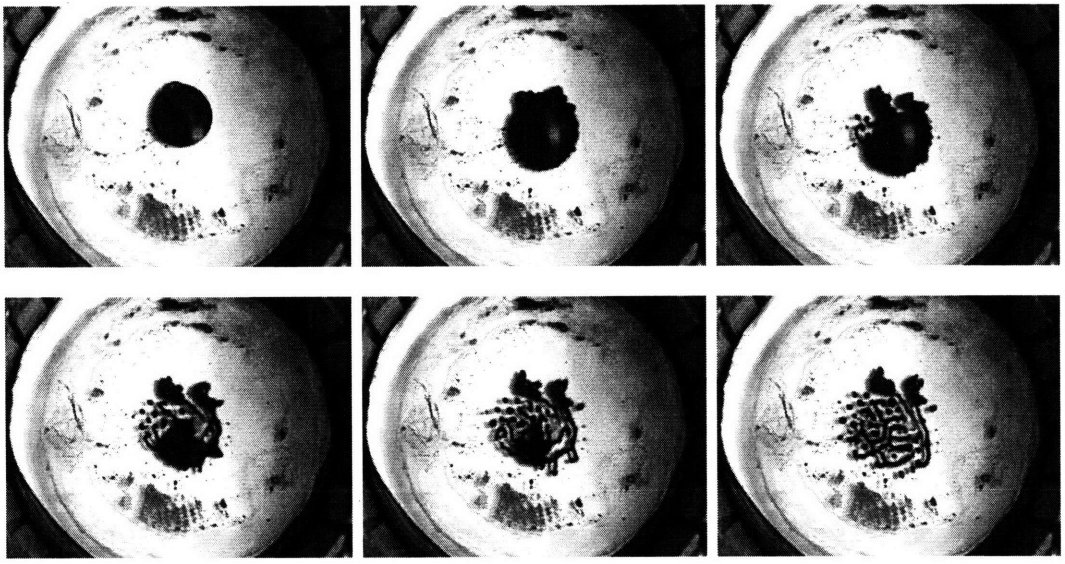

Figure 4-27: Sequence of phase transition patterns. The stator coil winding is excited to produce a 35 Hz, 31.7 Gauss CW rotating magnetic field. The 3134 Gauss permanent magnet is slowly brought toward the Hele-Shaw cell to a final critical distance of 4.2 cm to provide the axial DC magnetic field.

Chapter 5

Concluding Remarks

This work has focused on resolving discrepancies in earlier work on the direction of rotating magnetic fields and to determine if the polarity of the DC magnetic field has any effect on ferrofluid patterns. A second focus of this work was to use a small Magswitch permanent magnet to replace a large and bulky electromagnet and power supply. Previous reports [5][6] were uncertain on how the direction of rotation of rotating in-plane magnetic fields affects the orientation of the spirals formed by the ferrofluid after a DC axial field is applied. Measurements were taken with vertical positive and negative magnetic fields and with horizontal clockwise and counterclockwise rotating magnetic fields. The results showed that when the labyrinth pattern is formed from the vertical DC magnetic field, the spirals curl in the same direction as the rotating magnetic field and that the polarity of the axial DC field has no effect on the direction in which the spirals curl.

A Magswitch permanent magnet was also used to provide the DC axial field in the measurements in this thesis in order to replace large, non-portable electromagnet equipment for creating DC magnetic fields. The Magswitch magnet is small and compact and does not require any external power source. Using this magnet provides a portable solution to creating an axial DC field. Measurements were made of the three dimensional profile of magnetic fields at different heights and locations above the magnet. A reasonable region of uniform magnetic field was found that allowed ferrofluid spiral and dot patterns to form.

Many images were taken of the labyrinth patterns and the phase transitions using the Magswitch magnets as the DC magnetic field source. The resulting patterns were similar to those using the large bulky electromagnet system. Comparing these images to those obtained with the large equipment, it can be seen that the Magswitch magnet is a suitable replacement to the electromagnet to provide the axial DC field while still obtaining similar results.

Future work should find a lighter and more compact source for the rotating magnetic field. One company, ClickAutomation [8] makes small motors that may be a light and compact replacement. The rotor can be removed from these motors and the stator winding can be used to provide the rotating magnetic field.

Appendix A

Measurements with Magswitch Magnet Inside Stator

The following tables show the measured x, y and z components (B_x,B_y,B_z) of the magnetic field at different positions and heights above the top of Magswitch magnet using the original $\frac{1}{4}$ in thick, 50 mm diameter top and the constructed $\frac{3}{8}$ in thick, 3 in diameter top All measurements were taken with the Magswitch magnet inside the stator.

Table A.1: Measured x, y and z components (B_x,B_y,B_z) of the magnetic field at different positions and heights above the top of Magswitch magnet using the $\frac{3}{8}$ in thick, 50 mm diameter top. All measurements are in units of Gauss and were taken with the Magswitch magnet inside the stator.

	z, Height above Magnet (cm)																	
	0			1			2			3			4			5		
	B_x	B_y	B_z	B_x	B_y	B_z	B_x	B_y	B_z	B_x	B_y	B_z	B_x	B_y	B_z	B_x	B_y	B_z
A	-24.48	0.94	403.17	-18.92	10.80	343.05	-11.39	11.23	231.83	-5.10	9.72	140.20	-1.42	7.80	82.51	0.58	6.35	50.03
B	121.33	26.24	689.55	153.94	27.58	355.89	101.04	20.67	185.12	58.24	14.22	97.81	33.56	10.07	55.94	18.42	7.34	33.91
C	163.32	-189.75	762.39	111.95	-97.94	305.16	62.91	-40.47	169.19	36.61	-20.92	98.40	21.30	-9.42	58.80	12.02	-2.49	36.24
D	-38.54	-277.01	729.97	-30.15	-152.54	302.39	-23.01	-72.85	161.43	-13.74	-37.17	92.82	-6.97	-17.74	54.90	-2.50	-6.75	34.54
E	-238.49	-199.67	690.84	-120.32	-113.57	270.74	-66.82	-63.09	151.14	-35.66	-32.55	86.12	-18.50	-15.87	51.66	-8.05	-5.75	32.38
F	-401.01	14.77	761.76	-216.00	19.75	282.46	-121.27	15.71	140.22	-64.51	11.30	72.93	-33.29	8.46	40.75	-14.62	6.42	24.51
G	-366.85	253.2	648.61	-188.38	142.80	258.34	-98.71	79.61	118.82	-55.83	48.44	65.67	-27.08	27.24	35.04	-12.10	15.93	21.93
H	-65.39	401.66	840.95	-52.90	232.31	313.78	-31.32	132.11	131.63	-16.32	73.92	64.07	-7.29	40.86	33.83	-1.98	21.67	19.71
I	164.55	278.35	809.32	113.13	183.77	312.34	62.10	105.87	140.42	35.65	62.24	73.51	19.94	35.23	39.24	10.77	18.95	22.79
J	9.38	9.03	391.93	38.14	26.97	315.80	34.60	25.28	197.85	22.86	19.25	116.44	13.76	13.47	66.39	8.36	9.45	39.98
K	0.05	-18.12	385.99	22.92	-29.13	313.19	24.53	-21.34	200.79	17.48	-9.87	115.86	11.49	-3.03	69.08	7.40	0.81	41.36
L	-20.00	-40.04	397.91	-18.28	-53.73	311.21	-10.94	-41.55	198.35	-5.20	-23.23	116.79	-1.59	-10.50	67.96	0.47	-3.06	40.93
M	-58.33	-29.47	407.28	-74.18	-45.99	310.02	-50.41	-34.49	184.72	-28.05	-19.21	106.66	-14.20	-8.58	62.10	-5.95	-2.22	37.78
N	-65.66	6.30	392.75	-87.54	22.74	303.03	-66.25	22.29	191.48	-37.74	16.92	106.56	-19.83	12.05	61.13	-8.98	8.64	37.08
O	-64.03	38.97	421.67	-79.58	80.20	312.01	-52.83	65.05	177.11	-28.55	41.93	96.48	-14.33	25.98	54.75	-6.09	15.92	33.38
P	-29.29	39.93	395.11	-29.02	84.57	304.48	-19.63	67.32	182.45	-10.78	43.47	103.38	-5.13	27.46	61.47	-1.17	15.90	35.32
Q	73.45	25.00	367.96	19.19	59.20	295.85	18.56	49.82	182.05	12.62	33.78	104.86	8.23	21.47	60.42	5.31	13.75	36.56

Table A.2: Measured x, y and z components (B_x,B_y,B_z) of the magnetic field at different positions and heights above the top of Magswitch magnet using the $\frac{1}{4}$ in thick, 3 in diameter top. All measurements are in units of Gauss and were taken with the Magswitch magnet inside the stator.

	z, Height above Magnet (cm)																
	0			1			2			3			4			5	
	B_x	B_y	B_z	B_x	B_y	B_z	B_x	B_y	B_z	B_x	B_y	B_z	B_x	B_y	B_z	B_x	B_y	B_z
A	-7.51	7.51	222.24	-9.90	11.06	191.23	-7.00	10.48	138.70	-3.55	8.73	89.31	-1.45	7.30	55.78	0.88	6.02	37.33
B	112.40	9.88	496.43	143.92	31.26	223.21	90.58	22.98	82.72	52.58	15.91	37.77	28.54	10.86	18.26	14.61	7.42	10.16
C	189.32	-118.79	604.15	163.00	-82.64	173.53	85.65	-36.25	52.78	46.44	-17.07	24.61	25.12	-6.27	12.65	12.89	-0.32	8.08
D	30.42	-288.54	593.84	39.09	-204.06	167.18	22.05	-95.04	47.36	12.78	-45.17	20.52	8.00	-21.35	11.27	5.35	-7.53	7.21
E	-265.72	-195.88	508.37	-158.81	-142.75	156.37	-69.44	-66.60	40.09	-32.70	-31.27	17.24	-15.13	-14.09	9.12	-4.80	-4.02	6.22
F	-347.56	-21.91	645.41	-247.45	-2.09	134.34	-100.14	2.20	29.31	-47.28	3.27	12.91	-22.05	3.71	6.89	-7.77	3.97	4.95
G	-285.08	153.55	643.50	-189.50	140.36	139.95	-76.71	65.20	31.77	-35.50	34.33	13.79	-16.18	19.61	7.31	-4.77	10.81	5.19
H	-28.40	172.65	543.41	-7.56	191.84	211.11	-1.11	101.94	70.09	1.14	53.28	30.81	2.17	29.43	16.74	2.72	15.65	10.58
I	156.12	190.43	635.47	134.89	113.67	208.51	84.14	60.24	80.94	45.28	31.62	38.64	24.80	18.19	23.11	13.52	10.84	15.29
J	16.24	-8.21	273.73	61.25	-5.84	209.60	55.28	-1.62	121.31	36.57	1.07	66.32	21.82	2.50	38.01	11.86	3.27	23.91
K	9.99	-32.03	280.52	42.84	-58.46	207.36	39.20	-44.17	117.36	26.32	-25.27	63.25	15.95	-11.98	36.07	9.04	-3.66	22.96
L	-11.76	-29.26	251.43	-6.93	-58.89	195.33	-2.67	-49.41	118.99	-0.11	-30.97	69.29	1.01	-15.92	40.37	1.86	-5.85	25.65
M	-30.69	-26.05	260.33	-50.10	-48.54	199.04	-40.34	-41.01	118.26	-25.01	-24.80	65.95	-12.47	-12.32	37.93	-4.52	-4.03	24.07
N	-44.85	-3.45	267.58	-84.45	4.15	205.97	-67.57	6.43	119.21	-39.77	6.19	63.21	-20.71	5.49	35.29	-8.25	4.71	22.23
O	-25.59	8.37	242.18	-42.80	32.63	198.82	-36.62	33.77	127.36	-23.43	25.12	75.65	-11.86	16.25	43.35	-4.57	10.22	27.37
P	-6.54	21.66	263.26	0.62	62.76	206.79	3.81	56.71	124.58	4.07	38.64	71.09	3.66	23.76	40.90	3.27	13.47	25.40
Q	7.68	11.04	255.32	33.07	37.39	205.39	33.19	36.03	129.73	23.58	25.45	74.48	14.85	16.26	43.22	8.86	9.95	26.98

Appendix B

Measurements with Magswitch Magnet in Free Space

The following tables show the measured x, y and z components (B_x,B_y,B_z) of the magnetic field at different positions and heights above the top of Magswitch magnet using the original $\frac{1}{4}$ in thick, 50 mm diameter top and the constructed $\frac{3}{8}$ in thick, 3 in diameter top All measurements were taken with the Magswitch magnet in free space.

Table B.1: Measured x, y and z components (B_x,B_y,B_z) of the magnetic field at different positions and heights above the top of Magswitch magnet using the $\frac{3}{8}$ in thick, 50 mm diameter top. All measurements are in units of Gauss and were taken with the Magswitch magnet in free space.

	z, Height above Magnet (cm)																	
	0			1			2			3			4			5		
	B_x	B_y	B_z	B_x	B_y	B_z	B_x	B_y	B_z	B_x	B_y	B_z	B_x	B_y	B_z	B_x	B_y	B_z
A	-26.65	15.27	394.13	-22.20	14.85	333.54	-13.54	12.80	245.81	-6.23	12.11	167.96	-2.97	7.97	116.36	-2.24	6.76	82.50
B	100.44	49.03	620.90	136.60	30.28	315.36	85.71	20.25	199.36	53.15	13.93	134.86	35.03	12.62	95.04	23.77	9.85	70.25
C	71.45	-84.08	613.15	91.26	-71.56	334.59	64.96	-47.02	204.05	39.93	-25.69	139.07	29.13	-14.00	95.70	19.23	-9.44	69.85
D	-12.47	-150.30	634.34	-6.50	-129.48	329.24	-4.65	-83.30	204.68	-1.14	-48.76	137.78	3.05	-29.62	96.83	2.53	-18.10	70.47
E	-131.16	-119.65	634.70	-123.91	-97.52	313.32	-66.87	-61.08	204.93	-42.50	-37.56	133.00	-23.13	-22.82	96.96	-14.88	-13.29	70.31
F	-279.35	-40.44	665.75	-171.61	-4.18	306.15	-103.93	-0.85	193.93	-61.98	-1.51	132.04	-38.16	1.92	94.73	-23.80	1.64	70.01
G	-223.53	131.53	664.94	106.63	-145.88	296.95	-86.95	65.18	192.74	-52.35	43.04	129.17	-31.65	29.05	93.63	-19.80	19.45	70.14
H	-68.40	203.76	648.50	-34.14	163.06	310.57	-19.78	102.44	197.67	-11.27	64.29	133.73	-6.92	42.51	95.38	-3.58	30.79	68.29
I	81.95	235.56	702.23	73.35	129.51	319.16	50.11	80.48	200.37	35.55	46.36	136.03	20.96	33.64	96.60	16.96	23.43	69.27
J	9.27	22.28	443.36	51.43	25.83	346.26	44.19	14.88	236.08	28.90	14.04	158.09	18.16	12.60	110.28	15.85	9.23	77.24
K	3.96	-5.84	443.44	38.56	-30.45	346.43	35.74	-24.61	235.50	18.19	-14.61	159.84	15.13	-6.93	109.98	11.87	-2.69	78.26
L	-22.68	-25.32	446.92	-13.62	-67.11	344.78	-7.18	-52.31	232.34	-5.76	-29.79	156.64	-1.43	-18.83	107.87	0.39	-8.56	78.61
M	-52.15	-15.02	441.32	-66.00	-39.94	340.32	-45.01	-34.09	234.18	-29.66	-20.38	156.47	-18.27	-13.22	107.71	-9.72	-7.33	77.52
N	-66.49	11.86	435.06	-92.45	9.44	337.41	-71.37	2.56	229.46	-43.37	4.48	154.86	-24.94	3.17	109.19	-15.00	4.12	78.36
O	-65.80	40.86	448.23	-84.81	56.30	337.18	-60.66	45.63	228.63	-34.32	29.50	156.14	-21.35	23.49	107.19	-12.36	15.96	77.72
P	-34.79	66.61	461.93	-27.93	98.08	339.71	-22.93	69.07	229.95	-12.27	44.00	155.78	-5.34	33.07	106.11	-2.63	20.68	78.11
Q	-2.13	58.92	460.90	28.36	77.15	343.63	24.48	55.74	233.18	14.06	36.23	157.74	11.37	24.21	109.43	11.16	17.43	77.24

Table B.2: Measured x, y and z components (B_x,B_y,B_z) of the magnetic field at different positions and heights above the top of Magswitch magnet using the $\frac{1}{4}$ in thick, 3 in diameter top. All measurements are in units of Gauss and were taken with the Magswitch magnet in free space.

	z, Height above Magnet (cm)																
	0			1			2			3			4			5		
	B_x	B_y	B_z	B_x	B_y	B_z	B_x	B_y	B_z	B_x	B_y	B_z	B_x	B_y	B_z	B_x	B_y	B_z
A	-13.30	9.32	198.27	-9.10	6.88	175.57	-5.17	7.66	147.24	-5.31	6.56	114.64	-0.58	5.60	85.53	-1.12	5.70	66.23
B	78.34	24.04	380.70	89.23	14.70	184.05	64.88	12.11	126.28	47.18	11.43	89.31	34.70	9.97	63.28	24.89	8.40	52.53
C	44.79	-54.51	360.33	64.81	-56.59	187.29	49.80	-39.42	124.51	36.15	-26.39	88.05	26.45	-16.27	64.36	20.29	-11.16	50.23
D	-22.36	-91.95	367.77	-3.21	-92.78	179.59	0.62	-64.52	121.30	3.33	-42.00	88.99	2.43	-27.22	65.03	2.74	-18.86	51.58
E	-94.37	-75.63	365.01	-65.19	-73.10	173.02	-41.74	-51.39	121.42	-30.80	-32.97	87.08	-19.06	-22.14	64.44	-14.36	-14.63	49.72
F	-155.18	-5.22	354.47	-109.59	-7.22	166.24	-72.29	-1.25	119.93	-49.42	-2.09	86.02	-32.89	-0.48	63.47	-23.50	0.81	50.04
G	-128.34	85.51	365.54	-94.72	69.74	159.03	-62.71	51.33	119.93	-39.01	37.84	84.99	-27.91	26.65	60.20	-19.25	22.04	47.16
H	-46.99	129.34	361.00	-27.87	109.97	165.57	-14.31	77.11	110.15	-8.19	54.43	86.31	-2.80	39.76	62.37	-3.47	30.47	48.59
I	32.50	121.39	364.65	51.13	92.57	173.49	35.54	65.44	117.29	27.54	45.71	86.77	19.54	33.66	63.03	14.87	25.96	50.22
J	6.12	11.79	229.85	28.43	11.71	188.78	32.76	9.93	120.50	28.37	8.90	107.82	20.96	7.82	79.03	15.95	6.83	61.50
K	2.44	-3.92	234.44	17.84	-18.47	189.18	22.38	-16.32	146.40	21.13	-13.50	108.09	15.64	-8.67	78.99	12.75	-4.65	61.21
L	-13.29	-7.71	223.99	-10.03	-31.81	187.31	-2.49	-30.03	147.17	1.03	-23.51	107.87	1.66	-15.63	78.83	3.01	-9.48	61.57
M	-27.71	-6.63	227.77	-33.52	-24.30	184.24	-29.87	-28.19	141.50	-23.19	-20.50	104.31	-13.41	-13.87	77.00	-7.70	-8.38	60.74
N	-36.88	7.45	225.64	-51.63	1.25	182.00	-42.64	-0.08	141.62	-33.54	1.65	105.08	-23.88	2.28	76.50	-16.35	2.46	59.71
O	-29.45	22.41	221.77	-43.29	32.34	181.57	-37.49	31.81	140.34	-28.08	25.90	104.38	-20.67	21.92	74.34	-12.39	16.12	60.01
P	-17.30	34.91	232.71	-15.46	51.73	184.09	-14.06	48.28	141.06	-8.42	38.85	104.47	-5.31	29.84	75.75	-1.24	23.33	59.08
Q	0.02	32.10	237.53	18.05	43.94	187.88	17.34	39.70	144.18	15.98	32.78	106.06	11.84	24.57	77.86	11.91	18.39	59.94

Bibliography

[1] Rinaldi, C., A. Chaves, S. Elborai, X. He, and M. Zahn, Magnetic Fluid Rheology and Flows, Current Opinion in Colloid and Interface Science, 2005, 10, 141-157.

[2] Pankhurst, Q. A., J. Connolly, S. K. Jones, and J. Dobson, Applications of Magnetic Nanoparticles in Biomedicine, Journal of Physics D:Applied Physics, 2003, 36, 167-181.

[3] Bradley, William G. Fundamentals of MRI: Part II [Online]. [November 28, 2005]. Available from World Wide Web : <http://www.e-radiography.net/mrict/fund%20mr2/fundmri%202.htm>.

[4] Zahn, M and E.Adalsteinsson, Systems and Methods for Tuning Properties Nanoparticles, Provisional patent filed September 21, 2005; application no. 60/719,681.

[5] Lorenz, C. and M. Zahn, Hele-Shaw Ferrohydrodynamics for Rotating and DC Magnetic Fields, American Physical Society, Division of Fluid Dynamics, 2003 Gallery of Fluid Motion; Physics of Fluids Gallery of Fluid Motion, Vol. 15, No. 9, Sept. 2003.

[6] Rhodes, S., X. He, S. Elborai, S.-H. Lee, and M. Zahn, Magnetic Fluid Behavior in Uniform DC, AC, and Rotating Magnetic Fields, Journal of Electrostatics, 2006, Vol. 64, pp. 513-519.

[7] Magswitch magnets - switchable magnetic devices. 2007. Magswitch. <http://www.magswitch.com.au>.

[8] ClickAutomation.com - for all your automation needs. 2004. ClickAutomation. <www.clickautomation.com>.